

1 Moss kill-dates and modeled summer temperature track episodic snowline lowering
2 and ice-cap expansion in Arctic Canada through the Common Era
3

4 ^{1,2}Gifford H. Miller, ³Simon L. Pendleton, ^{1,4}Alexandra Jahn, ⁵Yafang Zhong, ¹John T. Andrews, ¹Scott
5 J. Lehman, ⁶Jason P. Briner, ^{1,2}Jonathan H. Raberg, ⁷Helga Bueltmann, ⁸Martha Reynolds, ⁹Áslaug
6 Geirsdóttir, and ¹⁰John R. Southon

7
8 ¹Institute of Arctic and Alpine Research University of Colorado Boulder, Boulder, CO 80303, USA

9 ²Department of Geological Sciences, University of Colorado Boulder, Boulder, CO 80303, USA

10 ³Environmental Science and Policy Program, Plymouth State University, Plymouth, NH 03264, USA

11 ⁴Department of Atmospheric and Oceanic Sciences, University of Colorado Boulder, Boulder, CO 80303, USA

12 ⁵Space Science & Engineering Center, University of Wisconsin-Madison, Madison, WI 53706, USA.

13 ⁶Department of Geology, University at Buffalo, Buffalo, NY, USA

14 ⁷Institute of Biology and Biotechnology of Plants, University of Münster, Münster, Germany

15 ⁸Institute of Arctic Biology, University of Alaska Fairbanks, Fairbanks, AK, USA

16 ⁹Institute of Earth Sciences and Department of Earth Sciences, University of Iceland, Reykjavik 101, Iceland

17 ¹⁰W.M. Keck Carbon Cycle AMS Laboratory, University of California at Irvine, Irvine, CA, USA
18

19 **Correspondence to:** Gifford H. Miller (gmiller@colorado.edu)
20
21

22 **ABSTRACT**
23

24 Most extant ice caps mantling low-relief Arctic Canada landscapes remained cold-based throughout
25 the late Holocene, preserving *in situ* bryophytes killed as ice expanded across vegetated landscapes.
26 After reaching peak late Holocene dimensions ~1900 CE, ice caps receded as Arctic summers
27 warmed, exposing entombed vegetation. The calibrated radiocarbon ages of entombed moss
28 collected near ice-cap margins (kill-dates) define when ice advanced across the site, killing the
29 moss, and remained over the site until the year of their collection. In an earlier study we reported
30 94 Last Millennium radiocarbon dates on *in situ* dead moss collected at ice-cap margins across
31 Baffin Island, Arctic Canada. Tight clustering of those ages indicated an abrupt onset of the Little
32 Ice Age ~1240 CE, and further expansion ~1480 CE, coincident with episodes of major explosive
33 volcanism. Here we test the confidence in kill dates as reliable predictors of expanding ice caps by
34 re-sampling two previously densely sampled ice complexes ~15 years later, after ~250 m of ice
35 recession. The probability density functions (PDF) of the more recent series of ages matches PDFs
36 of the earlier series, but with a larger fraction of early CE ages. Post 2005 CE ice recession has
37 exposed relict ice caps that grew during earlier Common Era advances and were preserved beneath
38 later ice-cap growth. We compare the 107 kill dates from the two ice complexes with 79 kill dates
39 from 62 other ice caps within 250 km of the two densely sampled ice complexes. The PDF of kill
40 dates from the 62 other ice caps cluster in the same time windows as those from the two ice
41 complexes alone, with the PDF of all 186 kill dates documenting episodes of widespread ice
42 expansion restricted almost exclusively to 250-450 CE, 850-1000 CE and a dense early Little Ice Age
43 cluster with peaks at ~1240 and ~1480 CE. Ice continued to expand after 1480 CE, reaching

44 maximum dimensions ~1880 CE, still visible as zones of sparse vegetation cover in remotely sensed
45 imagery. Intervals of widespread ice-cap expansion coincide with persistent decreases in mean
46 summer surface air temperature for the region in a Community Earth System Model (CESM) fully
47 coupled Common Era simulation, suggesting primary forcing of the observed snowline lowerings
48 were both modest declines in summer insolation, and cooling resulting from explosive volcanism,
49 most likely intensified by positive feedbacks from increased snow-cover and sea-ice and reduced
50 northward heat transport by the oceans. The clusters of ice-cap expansion defined by moss kill-
51 dates are mirrored in an annually resolved Common Era record of ice-cap dimensions in Iceland,
52 suggesting this is a circum-North-Atlantic-Arctic climate signal for the Common Era. During the
53 coldest century of the Common Era, 1780-1880 CE, ice caps mantled >11,000 km² of north-central
54 Baffin Island, whereas <100 km² is glaciated at present. The peak Little Ice Age state approached
55 conditions expected during the inception phase of an ice age and was only reversed after 1880 CE
56 by anthropogenic alterations of the planetary energy balance.

57

58 **1. INTRODUCTION**

59

60 The Canadian Arctic Archipelago (CAA) supports nearly 150,000 km² of glaciers and independent
61 ice caps, the greatest concentration of land ice outside Greenland and Antarctica (Medrzycka et al.,
62 2022). As Earth warms, regardless of forcing mechanism, strong positive feedbacks in the Arctic
63 result in greater temperature increases there relative to the planetary average on all timescales
64 (Miller et al., 2010). Consistent with that, the rate of contemporary warming for the Arctic is greater
65 than for most other geographic regions (Rantanen et al., 2022), particularly across the North
66 Atlantic sector (Zhong et al., 2018). All CAA glaciers are now losing mass as summers continue to
67 warm (Gardner et al., 2012; Lenaerts et al., 2013; Noël et al., 2018). In a review of controls on glacier
68 mass balance in the CAA, Koerner (2005) demonstrated that summer temperature explains ~95%
69 of annual mass balance variations over the previous 40 years of record, with the winter mass
70 balance having negligible explanatory power. Consequently, changes in glacier dimensions
71 dominantly reflect changes in summer temperature, and changes in glacier dimensions over time
72 provide one of the most reliable records for the evolution of past summer temperatures. Unlike
73 biological proxies that require evaluating an organism's adaptations that mitigate climate stressors,
74 glaciers have no strategy for survival. If it snows more in winter than melts in summer, non-calving
75 glaciers expand; conversely, if more mass is lost by summer melt than is gained through winter
76 snowfall, they recede.

77 Baffin Island, largest island in the CAA, is an elongate tilted Precambrian block, stretching
78 ~1600 km paralleling the west coast of Greenland. The island was inundated by the Laurentide Ice
79 Sheet (LIS) at the last glacial maximum. Although deglaciation proceeded rapidly under high
80 summer insolation in the early Holocene, our field area (Fig. 1), remained beneath the residual ice
81 sheet 7000 years ago, and probably was not free of Laurentide ice until after 5 ka (Dyke, 2004). The
82 Barnes Ice Cap, at the southern edge of our field area, is a remnant of the LIS, and the coastal
83 highlands east of our field area never fully deglaciated in the Holocene (Pendleton et al., 2019a).

84 Our primary focus is the 30,000 km² north-central uplands inscribed in Fig. 1, which rise
85 gradually from sea level at the west coast to ~900 m asl inland, after which the land rise rapidly to
86 the high-elevation, deeply dissected fiord country along the east coast, where the interfluves are
87 mantled by large ice caps and cirque glaciers. In contrast, isolated small, thin ice caps currently
88 cover ~100 km² of the highest summits across the low-relief uplands. Vegetation is sparse,
89 dominated by lichens and bryophytes, with less common vascular plants. The only woody plants
90 are prostrate species of willow (*Salix*). Our sampled ice caps (Fig. 1) occur across a larger region of
91 about 55,000 km².

92

93 **2. NEOGLACIATION**

94

95 Although deglaciation of the Laurentide Ice Sheet from Baffin Island continued through most of the
96 Holocene, the orbitally driven decline of Northern Hemisphere summer insolation after ~11 ka
97 resulted in a gradual lowering of snowline and high-elevation ice-cap expansion as early as 9 ka
98 (Lecavalier et al., 2017; Pendleton et al., 2017). Local ice cap and cirque glaciers were advancing by
99 5 ka (Moore et al., 2001), considered the onset of Neoglaciation, with ice expansion widespread by
100 ~3 ka (Miller, 1973). In response to the continuing decline in Northern Hemisphere summer
101 insolation, Baffin Island ice caps reached their maximum dimensions during the Little Ice Age (1240-
102 1900 CE), the coldest centuries of the Holocene (Miller et al., 2012). Initial dating of Neoglacial ice
103 margins was by lichenometry (Miller, 1973; Locke and Locke, 1977; Davis, 1985) and subsequently
104 based on cosmogenic isotopes in moraine boulders (Anderson, et al., 2008; Briner et al., 2009;
105 Crump et al., 2017). Continuous records of Neoglacial activity on Baffin Island are derived from lake
106 sediment cores (Moore et al., 2001; Miller et al., 2005; Briner et al., 2006; Briner et al., 2016), all
107 confirming maximum ice dimensions and/or summer cold during the Little Ice Age. Ives (1957;
108 1962) was the first to recognize that spectral differences in aerial imagery of northern Baffin Island
109 indicated that sparsely vegetated regions reflected a Little Ice Age (LIA) lowering of snowline that
110 killed all vegetation beneath the ice, and that early 20th Century warming had reduced an extensive
111 LIA ice complex to the few small remaining ice caps that mantle the highest summits (Williams,
112 1978). Wolken et al. (2005) evaluated the evidence for and against permanent ice cover explaining
113 the sparsely vegetated zones, concluding that permanent ice cover was indeed the most likely
114 cause. Although re-vegetation is rapidly occurring, the spectral signal remains preserved in recent
115 satellite imagery (Fig. 2), although less distinct than in imagery from the 1950s. Andrews et al.
116 (1975; 1976) used the light-toned areas on air photos and satellite imagery to produce the first map
117 of perennial ice-cover over north-central Baffin Island at the peak of the Little Ice Age. However,
118 dating of the LIA snowline minimum remained uncertain.

119 Falconer (1966) was the first to recognize that the receding upland ice caps were frozen to
120 their beds. Rather than active erosive agents, they are exceptional preservation agents. Bedrock
121 striae appearing as contemporary ice recedes show ice flow to the NE around all margins of current
122 ice caps, reflecting only regional Laurentide Ice Sheet flow at the last glacial maximum (LGM; Dyke,
123 2004). Striae, relict patterned ground (Falconer, 1966), delicately perched LGM erratic boulders
124 resting on NE-trending striae appearing as contemporary ice surfaces lower (Fig. 3), and the lack of

125 englacial debris, confirm cold-based ice. As ice caps recede, they also reveal entombed vegetation
126 in position of growth. The calibrated radiocarbon ages of dead moss (“kill dates”), define when ice
127 expanded across the site, killing vegetation, and then remained over the site, preserving the dead
128 plants until ice recession. Once exposed, dead vegetation is efficiently removed by meltwater or
129 wind-blown snow within a few years, although in rare settings devoid of meltwater, ice-killed
130 vegetation is known to survive intact for several decades (e.g., Miller et al., 2017; Pendleton et al.,
131 2017). Falconer (1966) reported the first radiocarbon date on *in situ* dead moss collected at the
132 margin of Tiger Ice Cap (Fig. 2), 330 ± 75 yr BP (I-1204), confirming ice expansion occurred during the
133 Little Ice Age, but the precision is too low to include here. Miller visited the same ice cap in 1981,
134 collecting moss at the ice edge that returned a ^{14}C age of 460 ± 25 (GSC-5025), early in the Little Ice
135 Age.

136 Here we report 186 calibrated radiocarbon dates on *in situ* dead moss collected at the
137 margins of receding ice caps that mantle summits across the uplands of northern Baffin Island,
138 including all 107 ice-marginal dates within the area inscribed in Fig. 1, and an additional 79 CE dates
139 from 62 other local glaciers and ice caps in the adjacent high-elevation mountainous regions (Fig.
140 1). We report kill-dates from two densely sampled ice-cap complexes, each sampled ~ 15 years
141 apart, and compare those ages with Common Era dates from 62 other ice caps within 250 km of
142 the densely sampled ice complexes. Three age clusters defined by the probability density functions
143 (PDF) of the composited 186 kill-dates are compared with mean summer temperatures simulated
144 in a fully coupled climate model for the Common Era (CESM past2k; Zhong et al., 2018). The kill-
145 date clusters correspond to century-scale anomalously cold summers in the model, whereas gaps
146 between kill-date clusters are relatively warm summers in the model. The close correspondence
147 between modeled summer temperatures and changes in ice-cap dimensions, allows us to constrain
148 the age of previously undated, low-elevation, sparsely vegetated zones that define an interval of
149 extensive ice-cap cover at elevations up to 400 m below extant ice cap margins.

150 151 **3. METHODS**

152
153 Beginning in 2005, we built on the pioneering work of Ives, Andrews, and Falconer, collecting *in situ*
154 dead moss, usually within a meter of the ice margin at the time of collection. We concentrated our
155 field studies on the low-relief upland of north-central Baffin Island between the Barnes Ice Cap and
156 Lancaster Sound (Fig. 1), with permission from the Qikiqtani Inuit licensed through the Nunavut
157 Research Institute. We densely sampled two ice complexes mantling the highest uplands: the
158 Serpens Ice Complex (SRP) consisting of three primary ice caps, and the Orion Ice Complex (ORN;
159 both unofficial names), consisting of six ice caps in 2005 (Fig. 2). Additional collections were made
160 in 2009, 2010, 2018, and 2019.

161 162 3.1 Radiocarbon dated moss.

163 Our primary data set is the radiocarbon ages of *in situ* ice-edge dead moss. Ice-margin retreat rates
164 were measured at ~ 10 m yr $^{-1}$, and vertical lowering ≥ 1 m yr $^{-1}$ (2006-2008 CE), confirming vegetation
165 collected a few meters from the ice margin was exposed during the year of collection. Regions

166 where similar studies use moss kill dates to reconstruct the timing of Neoglacial ice cap expansion
167 include Franz Josef Land (Lubinski et al., 1999), Svalbard (Miller et al. 2017), Greenland (Lowell et
168 al., 2013; Medford et al., 2021; Schweinsberg et al., 2017; 2018; Søndergaard et al., 2019), Baffin
169 Island (Falconer, 1966; Anderson et al., 2008; Miller et al., 2013; Margreth et al., 2014; Pendleton,
170 2019a&b), Alaska (Calkin and Ellis, 1981), Iceland (Harning et al., 2016), and Antarctica (Yu et al.,
171 2016; Groff et al., 2023).

172 We target members of the widespread moss family Polytrichaceae, primarily the genus
173 *Polytrichum*, which has a thickened central stem of sufficient mass that a single stem is adequate
174 for a precise AMS ^{14}C date. We previously showed that the ^{14}C concentration in living *Polytrichum*
175 is in equilibrium with that of the contemporary atmosphere, that ^{14}C dates on different *Polytrichum*
176 stems in a single clump are statistically indistinguishable, confirming that they grow relatively
177 quickly, and that ^{14}C dates on *Polytrichum* collected at four sites along 200 m of a modern ice cap
178 margin are statistically indistinguishable (Supplemental Fig. 1). These datasets support the
179 interpretation that the timing of ice-cap expansion can be reliably reconstructed from the ^{14}C kill
180 dates on *in situ* dead *Polytrichum* and other mosses revealed as ice caps recede under
181 contemporary warming. We note, however, that very different kill dates can occur over ice-margin
182 distances of a few tens of meters, when the receding ice margin intercepts a buried, older ice cap,
183 preserved beneath a more recent ice expansion (Fig. 4).

184 Although *Polytrichum* is the most common moss appearing as ice margins recede, if
185 *Polytrichum* is not present, we rely on *Andreaea*, a genus of small rock mosses that commonly grow
186 on siliceous rocks; they represent 9% of the dated samples. Because they are small, multiple strands
187 are required for dating. Another 30% of the dated samples were collected before we assigned
188 taxonomic names to moss collections; they are almost all likely to be Polytrichaceae. Radiocarbon
189 dates on co-located lichens are always older and are not included here. In the lab, plant samples
190 are sonicated in de-ionized water, then freeze-dried. From the freeze-dried samples sufficient
191 material (~2 mg) was separated and submitted for dating. Combustion and graphitization of
192 cleaned CO_2 is accomplished in INSTAAR's Laboratory for AMS Radiocarbon Preparation and
193 Research (NSRL) and measured at the W. M. Keck Carbon Cycle Accelerator Mass Spectrometry
194 Laboratory at the University of California, Irvine; a few samples were measured at the National
195 Ocean Sciences Accelerator Mass Spectrometry at Woods Hole Oceanographic Institution.
196 Radiocarbon dates were calibrated using OxCal 4.2.4 and IntCal20 (Bronk Ramsey, 2009; Reimer et
197 al., 2020) and expressed in years CE ($\pm 2\sigma$). Some of our dates were reported previously using
198 IntCal13, resulting in small changes in the calibrated age distributions in this paper. The OxCal
199 program reports the probability as a percentage for each year provided by the calibration process.
200 For collections of interest we sum the yearly probabilities, then normalize and plot as a probability
201 density function (PDF). Samples from multiple years and from different regions can be aggregated
202 and effectively compared this way. A complete tabulation of sample details and calibrated ages for
203 all 186 samples used in this report is available at the NSF Arctic Data Center
204 <https://arcticdata.io/catalog/view/doi:10.18739/A2RN30884>.

205

206 3.2 Climate Modeling

207 We make use of the CESM1-CAM5 (Hurrell et al., 2013) “past2k” transient climate simulation of the
208 Common Era (1-2005 CE; Zhong et al., 2018 GRL). This simulation has 2° resolution in the
209 atmosphere and land and ~1° resolution in the ocean and sea ice, the same configuration as used
210 for the CESM Last Millennium Ensemble (LME; Otto-Bliesner et al., 2016). The past2k forcing data
211 (Fig. 5) were mostly from the Paleoclimate Model Intercomparison Phase 4 project (PMIP4;
212 Jungclaus et al., 2017) for the Coupled Model Intercomparison Project Phase 6. They include
213 changes in solar irradiance and insolation, volcanic aerosols (Toohey et al., 2016), and greenhouse
214 gas levels (MacFarling et al., 2006). The land-cover forcing for the past2k simulation from 850 CE to
215 2005 CE is taken from the LME, which implements changes in grassland and cropland as compiled
216 by PMIP3. The land cover forcing from 1 to 849 CE is a superposition of HYDE3.1 cropland changes
217 (Goldewijk et al., 2011) onto the land cover forcing from the LME for 850 CE (see Zhong et al., 2018
218 for full details).

219 For us to assess the importance of anthropogenic activities in terminating the Little Ice Age,
220 we also use existing CESM1-CAM5 simulations at ~1° resolution in all model components for 1850-
221 2005 CE. Specifically, we make use of the simulated summer temperatures from four simulations
222 with all forcings (Hurrell et al. 2013), the standard “Historical” forcing used for the CESM1 CMIP5
223 simulations. We also use summer temperatures from three simulations with only “Natural”
224 forcings. The “Natural” forcing experiment is forced only by solar variability and volcanic aerosol
225 emissions, following the CMIP5 protocol (Taylor et al., 2012), and is part of a published dataset of
226 single forcing experiments with the CESM1-CAM for 1850-2005 that were previously used in other
227 studies (Meehl et al., 2020; Taylor et al., 2012; Xu et al. 2022). By using all available ensemble
228 members from these two experiments, we can assess the impact of the anthropogenic forcing
229 beyond the influence of internal variability.

230

231 **4. RESULTS**

232

233 4.1 Repeat sampling around the ORN and SRP ice complexes

234 In 2005 we collected dead moss around the margins of the Orion (ORN: 18 dated samples) and
235 Serpens (SRP: 22 dated samples, 4 collected in 2009) ice complexes (Fig. 2). The composite PDF of
236 both datasets showed similar kill date clusters (Miller et al., 2012). To test whether those clusters
237 were artifacts of the state of the ice caps during the year of collection, we re-sampled ORN in 2018,
238 and SRP in 2019, after ~250 m of ice recession at both, and with a greater sampling density.

239

240 4.1.1 Orion Ice Complex (Fig. 2) The 2005 moss kill-dates (Fig. 6A) cluster between
241 850 and 1000 CE and 1240 to 1480 CE, with a scattering of dates between the two clusters.
242 The PDF of 33 kill dates collected in 2018 (Fig. 6B) is broadly similar, with dominant clusters
243 between 850 and 1000 CE, and between 1240 and 1500 CE, but also an older cluster
244 between 250 and 450 CE. In the 2005-2018 composite PDF (Fig. 6C) the older cluster reflects
245 moss killed during an early First Millennium expansion of ORN, that likely melted partially
246 after 450 CE, but never completely disappeared. The residual early First Millennium ice cap
247 was subsumed by a late First Millennium expansion beginning ca. 850 CE, and preserved

248 beneath younger ice, only to re-emerge and re-start recession under contemporary warming,
249 exposing plants killed during the early First Millennium ice expansion. For example, where ice-
250 marginal moss produced early First Millennium ages at one of the ORN ice caps, the ice-surface
251 characteristics visible in high-resolution imagery captured for us by Digital Globe differ in character
252 from the glacier surface farther along the ice margin in either direction where the moss kill dates
253 are much younger (Fig. 4), supporting our interpretation that in 2018 a remnant early first
254 millennium ice cap that never melted completely was emerging from beneath a younger ice cap
255 that grew when snowline subsequently fell across the region. The near identical alignment of the
256 two younger 2018 clusters with those from 2005 confirms the utility of moss kill dates as reliable
257 ages of Common Era ice-cap expansion, regardless of collection date. A primary conclusion from
258 these data is that summer temperatures over the past century are warmer, on average, than any
259 century since 450 CE.

260

261 4.1.2 Serpens Ice Complex (Fig. 2) The PDFs of the 2005/2009 (22 dates) and 2019 (34 dates)
262 collections from SRP produce clusters in nearly identical time intervals 250 to 450 CE, 850 to 1000
263 CE and 1240 to 1480 CE (Fig. 7).

264

265 4.1.3 The SRP+ORN PDF (Fig. 8) The PDFs for all dates from SRP (Fig. 8A) and ORN (Fig. 8B)
266 are combined as a SRP+ORN composite (Fig. 8C), consisting of 107 calibrated ¹⁴C dates. That PDF
267 has three well-defined clusters, reflecting an early first millennium expansion between 250 and 450
268 CE found in 5 samples from SRP and 3 from ORN. There is virtually no evidence of ice expansion
269 between 450 and 850 CE, after which both ice complexes show expanding margins from 850 to
270 1000 CE (11 from ORN and 12 from SRP). ORN yielded 6 samples scattered between 1050 and 1160
271 CE, but with no central tendency, whereas SRP has none. However, both SRP and ORN have large
272 numbers of dates beginning ~1240 CE, and continuing until ~1480 CE (25 from ORN and 37 from
273 SRP), indicating ice margins expanded throughout that interval.

274 In both SRP and ORN composite PDFs (Fig. 8C) the sharply defined peak centered on ~780
275 CE is related to calibration. Radiocarbon ages between 1080 and 1180 yr BP have median calibrated
276 ages between 850 and 960 CE, but they all also have a low (<~5%) probability of an age clustered
277 tightly around 780 CE. Because 23 of the 109 radiocarbon dates from the two complexes are
278 between 1080 and 1180 yr BP, their calibration creates a low probability but strongly expressed
279 peak clustered tightly around 780 CE. Because of the low probability that this is the actual calibrated
280 age, and lacking other samples in the same time range, we consider it highly unlikely that 780 CE is
281 an interval of expanding ice caps.

282 We test the potential for variations in atmospheric ¹⁴CO₂ concentrations to have influenced
283 the structure of the SRP+ORN PDF (Fig. 8) by creating an artificial dataset of 186 samples (one every
284 8 calendar years), spanning the 1500-year interval covered by our dataset (1-1500 CE). We reverse-
285 calibrate those with the IntCal20 curve to derive a set of theoretical ¹⁴C ages - what the ¹⁴C ages
286 "should be" - but we take into account the fact that the measured ¹⁴C dates are not perfectly
287 accurate by modifying with sigma equal to 18 years, the average of our dating precision for the
288 moss ages. That modified set of simulated measured ¹⁴C ages is calibrated using the IntCal20 curve,

289 and the resulting probability distributions summed to quantify calibration bias (Fig. 9), which has
290 no pronounced peaks in the central clusters of kill dates shown in Figure 8, supporting our
291 contention that peaks in kill dates are a reliable estimate of expanding ice throughout the Common
292 Era.

293
294 4.1.4 Testing the SRP+ORN Composite (Fig. 10) The combined SRP+ORN PDF defines
295 sustained Common Era ice-cap expansion limited to three primary intervals: 250 to 450 CE, 850 to
296 1000 CE and after 1240 CE. The SRP Complex consists of 3 independent ice caps, whereas ORN
297 consisted of 6 independent ice caps sampled in 2005, of which portions of only 3 remain. To test
298 whether the densely sampled ice complexes reflect regional snowline lowering across northern
299 Baffin Island we collected 79 additional dead moss from the margins of 62 other ice caps. Those
300 additional ice caps include other small ice caps situated on low relief landscapes similar to ORN and
301 SRP, but also include low-relief summits within much larger ice complexes where ice-expansion is
302 primarily by vertical thickening rather than ice flow. None of the samples are from outlet glaciers;
303 all are within 250 km of SRP and ORN. We avoid cirque glaciers because response times to snowline
304 lowering are more complex than for small upland cold-based ice caps or the vertical thickening of
305 large ice caps, both of which change in direct response to summer temperature and are largely
306 unrelated to ice flow.

307 The resultant PDF of those 79 calibrated ages is compared with the PDF of the 107 dates
308 from SRP+ORN in Fig. 10. The isolated ice cap dates (Fig. 10B) cluster primarily in the same three
309 groupings apparent in the SRP+ORN PDF (Fig. 10A), although the early first millennium 250-450 CE
310 cluster is more strongly represented, and the onset extends to near the start of the First
311 Millennium. The three samples that contribute to that tail are from elevations above 900 m asl,
312 higher than ORN and SRP, suggesting that summer cooling began earlier than recorded by
313 SRP+ORN, and that snowline did not drop below 900 m asl until after 250 CE, or that subsequent
314 summer warmth fully melted all pre-CE advances. The 850-1000 CE cluster is apparent in both data
315 sets, and with similar overall structure, suggesting regional climate forcing. Both data sets lack
316 significant ice expansion between 1000 and 1240 CE, and both exhibit evidence of widespread
317 expansion beginning abruptly ~1240 CE and continuing to ~1480 CE.

318 The large cluster of kill-dates 1240-1480 CE suggest snowline declined throughout that
319 interval. However, at multiple sites ice-edge moss collected in 2005 with kill-dates ~1250 CE, are
320 older than ice-edge moss sampled in 2018 from sites orthogonal to the 2005 ice margin, with
321 younger kill dates (~1450 CE). The simplest explanation for this apparent contradiction is an interval
322 of modest ice recession after 1250 CE, followed by a readvance ~1450 CE, with preservation of the
323 older moss beyond the receded ice margin, which was re-covered during the ~1450 CE expansion.
324 This complex history of cold-based plateau ice caps advancing, receding, then re-advancing, can be
325 preserved in the ages of moss surviving multiple episodes of ice expansion. This is illustrated by the
326 three early First Millennium CE moss kill dates in Fig. 4 that are associated with ice of a different
327 character than adjacent ice with much younger moss kill dates. This requires a remnant early First
328 Millennium ice cap to have been subsumed by an interval of late First Millennium ice cap growth.
329 We conclude from the positions of moss with kill-dates between 1240 and 1480 CE that this 240-

330 year interval was not characterized by monotonic summer cooling; rather summer cooling
331 beginning ~1250 CE was interrupted by at least one episode of warm summers leading to modest
332 ice recession followed by re-expansion of the ice caps ~1450 CE.

333 The composite record consisting of 186 calibrated radiocarbon dates from 70 different ice
334 caps (Fig. 10C) constrains ice-cap expansion during the Common Era across northern Baffin Island.
335 The well-defined clusters suggest snowline began to decline early in the First Millennium CE,
336 resulting in widespread ice-cap expansion between 250 and 450 CE (21 dates). There is no evidence
337 from kill-dates for additional ice-cap growth until after 800 CE, with widespread ice-cap expansion
338 between 850 and 1000 CE (43 dates). Although there is little evidence for snowline lowering during
339 Medieval times, between 1000 and 1240 CE, summer temperatures were also not high enough to
340 melt all ice caps that formed in the first millennium. This suggests that Medieval times were
341 certainly not as warm, on average, as the earliest centuries of the Common Era, but also that
342 Medieval times experienced no sustained decades of significant summer cold. 1240 CE marks the
343 start of the Little Ice Age, with clear evidence of intermittent ice-cap expansion in all datasets,
344 continuing for the next 240 years (97 dates).

345 None of the kill-dates from plateau ice caps pre-date the Common Era. Consequently, if
346 earlier late Holocene episodes of summer cold resulted in long-lived ice caps across Baffin Island
347 uplands, subsequent summers were warm enough and/or long enough to completely melt those
348 ice caps before 1 CE. Our moss dates are relatively silent about the state of the ice caps after ~1500
349 CE. We turn to climate models to derive information on ice cap dimensions after 1500 CE

350

351 4.2 Modeling the evolution of Common Era summer temperature

352 From the past2k model output we extract simulated summer (JJA) 2-m air temperature averaged
353 over North Atlantic Arctic land areas (>60°N and between 90°W and 30°E) through the Common
354 Era (1-2005 CE), capturing a broad representation of North Atlantic Arctic lands, and including the
355 climate impacts from sea-ice feedbacks. Although climate is often approximated using a 30-year
356 average, cold-based ice caps mantling low-relief landscapes on Baffin Island have a longer, multi-
357 decadal response time, so we use a 50-year running mean for our data-model comparison. The 50-
358 year running mean of summer temperature through the Common Era exhibits a first-order declining
359 trend up to ~1890 CE (Fig. 11), consistent with declining NH summer insolation from orbital terms.
360 Because Baffin Island is only a portion of the land included in our extraction of mean JJA summer
361 temperatures (Fig. 11 Inset), the modeled temperatures are unlikely to match those of our field
362 area, and we evaluate the relative changes in summer temperature without regard to absolute
363 values.

364 To assess how well the past2k summer temperatures represent the summer temperature
365 evolution in the study region, we compare the past2k summer temperatures with a 50-year record
366 of summer temperature from the only Baffin Island interior weather station, Dewar Lakes, ~350 km
367 SE of our field area, at 500 m asl. The mean summer (JJA) temperature at Dewar Lakes from 1958-
368 2022 exhibits high inter-annual variability (up to 5°C, and a range of almost 9°C) but the 10-year
369 running mean (Fig. 12) shows that relatively warm summers in the 1950s were followed by colder
370 summers in the 1960s and early 1970s, after which variably warming summers dominate the

371 record. The 5-year running mean summer temperature record in our CESM past2k simulation for
372 the period of overlap (1958-2005; Fig. 12) reasonably mimics the Dewar Lakes record, when
373 accounting for the expected much lower variability in the model results due to the averaging over
374 a much larger area.

375 Both the Dewar Lakes recorded summer temperatures and CESM simulated summer
376 temperatures indicate cold summers in the 1960s and early 1970s. We compare those records with
377 ice-cap retreat rates for three ice caps (WT, SRP, ORN, Fig. 2) from remote images spanning 1957-
378 2020 CE. All three ice caps show reduced rates of aerial decrease between 1960 and the early 1970s
379 (Fig. 13), lending additional confidence in the simulated summer temperatures in the past2k results.
380 Summer warming in both Dewar Lakes and past2k records since 1980 is matched by increased ice-
381 cap recession rates. The close correspondence between past2k modeled summer temperatures the
382 Dewar Lakes recorded temperatures, and rates of ice-cap recession for WT, SRP, and ORN, provide
383 a measure of confidence in the CESM modeled summer temperatures through the Common Era.
384

385 4.3 Comparing modeled summer temperatures with ice-cap kill dates.

386 Because summer temperature is the dominant control on Baffin Island glacier mass balance
387 (Koerner, 2005) we expect below average modeled summer temperatures to correspond with
388 episodes of ice cap expansion. The modeled 50-year mean summer temperatures (Fig. 11) contains
389 significant centennial-scale structure. Primary forcings (Fig. 4) leading to the temperature decline
390 in the model include a reduction in Northern Hemisphere summer insolation through the Common
391 Era, small reductions in TSI between 1300 and 1700 CE, and episodes of sulfur-rich explosive
392 volcanism with the associated positive feedbacks from expanded sea ice, additional snow cover
393 over land, and changes in ocean circulation. Anthropogenic impacts become important after ~1850
394 CE.

395 A piecewise regression of JJA temperatures (1-1900 CE; Supplemental Figure 2) suggests an
396 initial steep decline from 1 to 900 CE, warming from 900 to 1050 CE, followed by a slower decline
397 between 1050 and 1900 CE. While the piecewise regression captures some of the Common Era
398 structure, it lacks the detail necessary to compare with the kill-date composite PDF (Fig. 10C).

399 To more directly compare past2k 50-year mean summer temperatures with the information
400 provided by our moss kill dates, we instead calculate multi-century linear regressions of modeled
401 summer temperature across time periods that kill-dates indicate involved wide-spread ice-cap
402 expansion, and across intervals lacking evidence of expanding ice caps (Fig. 11). This relaxes the
403 constraints for piecewise regressions that require individual regressions be continuous. The
404 regression through mean summer temperatures between 250 and 450 CE defines a steady decline
405 in summer temperature that accounts for ~25% of the modeled temperature decline between 1
406 and ~1880 CE. The modeled summer temperature decline is consistent with the earliest kill-date
407 cluster centered on 250-450 CE (Fig. 10C). The modest number of kill-dates between 1 and 250 CE
408 (Fig. 10C) are consistent with the onset of cooling summers 1-250 CE in the model, prior to the main
409 cluster of kill dates beginning at 250 CE.

410 Declining summer temperatures 250-450 CE were followed in the model by 50 years of
411 warmth before a 50-year strongly negative temperature excursion resulting from 536 CE explosive

412 volcanism (Büntgen et al., 2016) and associated positive feedbacks. A record of ice-cap expansion
413 at that time is not present in our kill dates. We presume snowline dropped and ice caps grew at this
414 time, but the short duration and rapid return to a century of relative warmth after the eruption
415 likely resulted in enough melt that evidence of 536 CE ice-cap expansion is lost.

416 High multi-decadal temperature variability without a trend between 450 and 800 CE is
417 predicted to result in changes in snowline, but because cold summers are brief (2 to 3 decades) and
418 followed by warm summers, development of persistent ice caps is unlikely, hence there are no kill
419 dates. However, a strong 100-year cooling trend between 840 and 940 CE produced the coldest
420 sustained temperatures of the First Millennium, and aligns with the second main kill-date cluster
421 between 850 and 1000 CE.

422 Modeled Medieval temperatures in our past2k simulation suggest high-magnitude
423 multidecadal variability between 950 and 1200 CE, but without a trend, and at a mean temperature
424 similar to the coldest decades around 400 CE. This is consistent with Medieval times not being warm
425 enough to fully melt ice caps that formed early in the First Millennium. However, the mean
426 Medieval summer temperature is warmer than summers during the 850-1000 CE ice expansion, in
427 conflict with the forty-two sites with kill-dates between 850 and 1000 CE that remained intact
428 through Medieval time. We suggest that either the late First Millennium CE summer temperatures
429 are too low, or modelled Medieval summer warmth is too high to be reconciled with strong the
430 cluster of dead veg ages 850-1000 CE; an explanation for this discrepancy remains unresolved.

431 From 1240 to 1880 CE summer temperatures decline overall in the model, consistent with
432 our kill dates and with the low snowline required by the elevations of sparsely vegetated lowlands
433 (Fig. 2). Finding ~1240 CE kill dates outboard of 1480 CE dates (section 4.1.4), requires a multi-
434 decadal oscillation of ice-cap dimensions (e.g., a ~1240 CE advance, followed by ice recession
435 without all dead moss eroded away, followed by a subsequent advance ~1480 that allowed ice caps
436 to re-cover moss killed in 1240 CE), and to also kill newly colonized moss both inboard and outboard
437 of the 1240 CE sites. This is consistent with modeled summer temperatures exhibiting significant
438 multi-decadal variability, but never warm enough or long enough to melt all ice that expanded
439 ~1240 CE, early in the Little Ice Age. The lack of kill dates younger than 1500 CE suggests it is unlikely
440 there was any century after 1500 CE with average summer temperatures higher than the 1240-
441 1480 CE mean until 20th Century warming, which is consistent with modeled summer temperatures
442 (Fig. 11).

443 Modeled summer temperature decreases after Medieval Times are a response to major
444 explosive volcanism ~1240 and ~1440 CE (40 and 50 years, respectively; Sigl et al., 2015). Eighteen
445 of 186 kill dates (Fig. 10C) have median calibrated ages between 1440 and 1480 CE, suggesting
446 widespread ice expansion then. The 97 sites with kill dates between 1240 and 1500 CE indicate
447 expansion of ice caps across those two centuries, consistent with large sulfur-rich volcanic
448 eruptions that produce a first-order declining trend in modeled summer temperatures.

449 There is broad agreement between modeled summer temperatures and the temporal
450 distribution of kill-dates, with the three primary clusters of kill dates centered on episodes of
451 centennial-scale declines in past2k modeled summer temperatures. The cluster of kill dates
452 between 1240 and 1480 CE align with the beginning of a 600-year irregular temperature decline in

453 modeled summer temperature, culminating in the coldest century of the Common Era between
454 1780 and 1880 CE. Rapid warming in the past2k model after ~1880 CE is consistent with rapid
455 cryosphere recession that reduced the ice-covered area across the northcentral Baffin Island
456 uplands from ~11,000 km² at the LIA maximum, to ~400 km² by 1960 CE, and <100 km² in 2022 CE.

457

458 **5. DISCUSSION**

459

460 5.1 Age of maximum Common Era ice-cap expansion

461 The swaths of sparsely vegetated regions across north-central Baffin Island first noted 70 years ago
462 (Ives, 1957) define the lowest persistent snowline of the Common Era, and represent peak cold of
463 the Little Ice Age (Ives, 1962; Andrews et al., 1975; 1976, Williams, 1978; Locke & Locke, 1977), but
464 independent dating of that interval has been elusive. To kill all vegetation requires multi-decadal
465 burial beneath ice. Because the regions that define peak LIA snowline lowering are discontinuous
466 (Fig. 2), more than 100 independent, cold-based ice caps, each a few tens of meters thick, and
467 ranging from ~50 km² to a few hundred km² in area must have mantled the currently sparsely
468 vegetated uplands during a century or more of coldest LIA summers. The spectral character along
469 the outer perimeters of the sparsely vegetated regions (Fig. 2) is mottled, suggesting a dominant
470 “permanent” ice cap over higher hills, and an outer perimeter where permanent snow lay in
471 landscape hollows long enough to kill vegetation, but not long enough to coalesce into the main ice
472 cap.

473 Although sparsely vegetated landscapes define the maximum dimensions of ice caps in the
474 Common Era, vegetation killed by that expansion was vulnerable to efficient removal by wind and
475 water erosion as ice caps receded. In 2005 we visited a “sparsely vegetated” region apparent in
476 remote imagery and found that re-vegetation was already advanced. We sampled a dead willow
477 (*Salix*) stem at 629 m asl, lower than any extant ice cap. The ¹⁴C age of the stem is “modern” (CURL-
478 7929: 1.16 FM), suggesting that vegetation killed by the lowest LIA snowline is rare or absent, and
479 little chance that radiocarbon can resolve when snowline reached its maximum LIA dimensions.

480 Recession of ice caps from regions defined by vegetation contrasts was nearly complete by
481 the middle of the 20th Century when remotely sensed imagery first became available. Because the
482 spectral contrast that defines the sparsely vegetated landscape in imagery from the 1950s is much
483 stronger than in contemporary imagery due to on-going re-vegetation, and because the sparsely
484 vegetated landscapes lack gradients in their spectral contrasts, ice recession from maximum LIA
485 dimensions must have been relatively rapid and continuous.

486 The youngest kill-dates are ~1500 CE, so the timing of maximum snowline lowering must
487 post-date 1500 CE. Having demonstrated that clusters of kill dates align with centuries of simulated
488 cold summers in the past2k simulation, and that past2k temperature trends align with the Dewar
489 Lakes summer temperature record of the past 50 years, we rely on the past2k simulation to
490 estimate the timing of peak snowline lowering defined by sparsely vegetated regions in remote
491 imagery. In the past2k simulation from 1500 to 2000 CE (Fig. 14) the irregular decline in summer
492 temperature reaches lowest values between 1780 and 1880 CE, the coldest century of the Common
493 Era. Subsequently, temperatures rose steadily to the warm decades of the 1930s - 1950s. We

494 conclude that the ice caps that killed vegetation apparent in remote imagery, persisted for at least
495 the 100 years of cold summers between 1780 and 1880 CE.

496

497 5.2 Comparing Baffin Island kill-date records with a continuous proxy record of ice-cap expansion 498 in Iceland through the Common Era

499 The composite PDF of 186 kill-dates from 70 ice caps (Fig. 10C) provides a direct record of past ice-
500 cap expansion, with changes in mean summer temperature the primary control on ice-cap
501 dimensions. A major advantage of our dataset is that moss kill-dates require no training sets for
502 their interpretation. Although they are discontinuous records, the discontinuities are important.
503 Consequently, they differ in significant ways from continuous records of glacier-dimension proxies.
504 To evaluate whether the Baffin kill-date record reflects the evolution of summer temperature for
505 the North Atlantic Arctic, as suggested by the strong correlation with climate model results for
506 those lands, we compare the discontinuous moss kill-date record that defines time of glacier
507 expansion on Baffin Island with a continuous, annually resolved Common Era record of glacier
508 dimensions from Iceland, also a part of the North Atlantic Arctic lands included in our model.

509 The Iceland record is derived from annual varve thicknesses in a sediment core from glacial
510 lake Hvítárvatn that drains Langjökull, the second largest ice cap in Iceland. Two primary Langjökull
511 outlet glaciers drain into the lake, and during the Little Ice Age, terminated in the lake. Varve
512 thicknesses are a direct measure of glacier dimensions; as the glacier grows, more erosion occurs,
513 and consequently, thicker annual sediment packets are recorded in Hvítárvatn. Because Hvítárvatn
514 freezes in winter, and Langjökull occupies easily eroded basaltic terrain, Hvítárvatn sediment is
515 characterized by high sedimentation rates and consequently measurable annual varve couplets for
516 the past 3000 years or more (Larsen et al., 2011).

517 The Hvítárvatn varve-thickness record over the Common Era is plotted against the moss kill-
518 date record in Fig. 15. Varve thicknesses are low, but easily measured, at the start of the Common
519 Era. There is a slight increase in varve thickness 250-450 CE, coincident with the first cluster of kill-
520 dates. A more prominent spike in varve thickness that occurs between 850 and 950 CE is coincident
521 with the second Baffin Island kill-date clusters between 850 and 1000 CE. The final kill-date cluster
522 (1240-1480 CE) is represented in the Hvítárvatn varve record by increasing varve thicknesses that
523 double between 1240 and 1480 CE. Our estimated age for the lowest Baffin Island snowline (1780-
524 1880 CE) is matched by Langjökull varves remaining relatively thick after 1480 CE until thickening
525 rapidly between 1780 and 1880 CE, when the outlet glaciers terminated in the lake (Larsen et al.,
526 2011). Although historical records confirm Langjökull has been receding since ~1900 CE, Hvítárvatn
527 varves remain thick because Langjökull is much thicker (~600 m) than Baffin Island upland ice caps,
528 so has a longer time constant when responding to large increases in summer temperature.

529 The commonalities between the Hvítárvatn varve thicknesses record as a proxy for
530 Langjökull dimensions and moss kill-dates representing episodes of Baffin Island ice cap expansion,
531 suggests both datasets provide a similar record of regional North Atlantic Arctic summer climate
532 through the Common Era. Most other Arctic Common Era summer temperature reconstructions
533 are pan-Arctic (e.g. McKay and Kaufman, 2014; Werner et al., 2018), and show summer
534 temperature variability through the First Millennium, but without a trend, which differs from our

535 records that show overall summer cooling through the same time interval. The difference is likely
536 because those records are pan-Arctic, whereas our results are limited to the North Atlantic Arctic
537 where the sea ice feedback is stronger, and climate modeling shows pan-arctic spatial gradients in
538 response to natural forcing over the Common Era (Zhong et al., 2018).

539

540 5.3 Evolution of Baffin Island snowline through the Common Era

541 The PDF of all moss kill-dates (Fig. 10C) defines three episodes of Common Era ice-cap expansion.
542 We derive an estimate of the corresponding snowline during each expansion from the mean
543 elevation of the lowest 20% of all dated sites for each interval. We define snowline as the lowest
544 elevation that snow or ice persisted long enough to kill all vegetation (multiple decades), sufficient
545 time for snow to turn into ice. During times of lowering snowline, ice margins expand at many
546 elevations. But because the ice caps are cold based and ice velocities are negligible, the lowest ice
547 margins are the closest quantitative estimate of snowline available. We recognize that ice cap
548 margins defined by their kill dates may be smaller than their maximum dimensions due to ice
549 recession before re-burial under a younger ice cap, but those elevations remain the best estimate
550 for the minimum snowline lowering. We estimate snowline at the peak Little Ice Age from the
551 lowest persistent elevation of remnant vegetation trimlines (Fig. 2), and assign an age of 1880 CE
552 to that snowline, as discussed in section 5.1.

553 During the Common Era snowline declined more than 400 m, from an initial elevation above
554 900 m asl to the sparsely vegetated hills 450 to 500 m asl. To evaluate how a declining snowline
555 elevation translates to the area of permanent ice, we calculate the distribution of area across
556 elevation for the region of low-vegetation cover outlined in Fig. 1. Reconstructed snowline
557 elevations for the three kill-date clusters are mapped on to the area/elevation relationship
558 (Supplemental Fig. 3). To calculate the area of permanent ice-cover at peak-LIA-cold, we measured
559 the area of sparsely vegetated regions (Supplemental Fig. 4). Fig. 16 illustrates the highly non-linear
560 relationship between snowline decline and resultant areal extent of permanent ice. Although we
561 lack quantitative snowline data between ice-cap advances, snowline could not have risen much
562 above the preceding low snowline for long or all ice from earlier advances would have melted and
563 no dead vegetation would have been preserved.

564

565 5.4 “Instantaneous glacierization” and the initiation of the Laurentide Ice Sheet

566 The large area of the north-central Baffin Island uplands ice covered at the peak of the Little Ice Age
567 relative to the area currently glacierized (e.g., Fig. 2) led to the concept of “Instantaneous
568 Glacierization” (Ives, 1957; Andrews et al., 1975; Ives et al., 1975) when a modest decline in
569 snowline can result in a dramatic increase in the area beneath ice caps. Subsequent simulations of
570 conditions leading to the initiation of the Laurentide Ice Sheet from an initial interglacial state (e.g.,
571 Andrews and Mahaffy, 1975; Clark et al., 1993; Kleman et al, 2002; Birch et al. 2017; 2018) all show
572 initial snow accumulation on Baffin Island with the albedo feedback providing an important
573 acceleration of ice-sheet growth.

574 The dramatic increase in the area under permanent snow/ice-cover in our field area
575 between 1480 and 1880 CE (Fig. 15), during which time snowline dropped 165 m, from ~665 to

576 ~500 m asl, is due to the large area of land between those two elevations (Supplemental Fig. 3).
577 Assuming a standard free air lapse rate of 0.6°C per 100 m, this drop in snowline required only a
578 1°C decrease in mean summer temperature. The direct evidence of “instantaneous glacierization”,
579 constrained by the limits provided by moss kill-dates and climate modeling illustrates how a
580 significant albedo increase may occur following a modest decrease in summer temperature, where
581 the resultant snowline descent results in a dramatic increase in permanently ice-covered lands.

582

583 5.5 Climate forcing that led to 20th Century ice-cap recession

584 The combination of direct evidence and modeled summer temperatures points to rapid recession
585 from maximum Common Era ice-cap coverage across north-central Baffin Island beginning in the
586 late 1800s CE. The past2k model simulates all summers after 1900 CE warmer than the mean
587 summer temperature of the 19th Century, with particularly warm summers between 1920 and 1960
588 CE (Figs. 14 and 16), similar to Arctic-wide temperatures in multiple climate model simulations with
589 all forcings (Fyfe et al., 2013). The dominant forcings that contribute to warming from 1900 to 1960,
590 by which time remote imagery shows that almost all peak LIA ice caps in the field area (Fig. 2) had
591 melted, include a slight increase in solar irradiance through the early 1900s, significant increases in
592 greenhouse gases (GHG: CO₂, CH₄, and N₂O; Fig. 4), partially compensated by a cooling effect from
593 increased anthropogenic aerosols and land-use change, and a very slight decline in Northern
594 Hemisphere summer insolation from orbital terms (e.g., Fyfe et al., 2013).

595 An underlying question is whether the cold century from 1780 to 1880 CE and resultant
596 dramatic increase in ice-covered terrain across north-central Baffin Island was the prelude to a
597 transition into a new ice age, or just an aberrant century that even without anthropogenic trace gas
598 inputs would have returned to warmer summers and ice-cap retreat. The primary impacts on
599 Earth’s planetary energy balance over the past century are the opposing effects of anthropogenic
600 aerosols and greenhouse gases, with modest impacts from solar irradiance and volcanism (Myhre
601 et al. 2013; Zhao et al. 2019).

602 Fyfe et al. (2013) compared pan-Arctic mean annual temperature anomalies over the 20th
603 Century in a range of models that included those using only “Natural” forcings (solar irradiance and
604 volcanism) and those using “Historical” forcings (Natural forcings plus greenhouse gas and aerosol
605 forcings). They found that “Natural” simulations resulted in no trend in circum-Arctic mean annual
606 temperatures, whereas “Historical” simulations produced a modest early 20th Century temperature
607 rise, a slight decline in temperature centered on the 1960s, and a steady warming thereafter.
608 However, the Fyfe et al. (2013) results cannot be compared in detail to our reconstructed changes
609 in the North Atlantic sector, which behave differently from the pan-Arctic average in paleoclimate
610 models (Zhong et al., 2018). Their conclusions also were for mean annual temperatures, whereas
611 we focus on mean summer temperature, the primary control on glacier mass balance (Koerner,
612 2005).

613 To test the potential role of anthropogenic forcing in the observed Baffin Island snowline
614 rise after 1880 CE we compare 15-year running means of summer (JJA) temperature over the North
615 Atlantic Arctic lands in a series of CESM1 ensembles beginning in 1850 CE with “Historical” (4 runs)
616 and CESM1 ensembles with only “Natural” forcings (3 runs; Hurrell et al. 2013, Meehl et al. 2020,

617 Xu et al 2022) in Fig. 17. The “Historical” and “Natural” ensembles track closely until ~1920 CE,
618 when the “Historical” ensemble continues a long increase in simulated summer temperature, with
619 a temporary reduction in the 1950s and 1960s, whereas the “Natural” forcing simulations fail to
620 show additional increases in summer temperature after 1920. Based on this comparison, it is likely
621 that some rise in snowline in the early 1990s would have occurred without any anthropogenic
622 disturbance in the planetary energy balance, but the significant increase in summer temperatures
623 after 1920 CE seen in both the past2k and “Historical” simulations is primarily a response to
624 anthropogenic impacts. This suggests that without Anthropogenic impacts, Baffin Island ice caps
625 would still be widespread at elevations well below 600 m asl, the lowest elevation ice cap in 1985
626 CE imagery (Fig. 2).

627

628 **6. CONCLUSIONS**

629

630 • Most ice caps mantling the cold, low-relief landscapes of Baffin Island are frozen to their beds,
631 allowing them to act as preservation agents. Ice cap dimensions are set by summer temperature,
632 with small changes in summer temperature driving significant changes in glacier dimensions. As
633 ice caps expand, they entomb vegetation *in situ*, preserving them until the vegetation is re-exposed
634 when ice caps recede. Radiocarbon dates on moss collected within a few meters of ice-cap margins
635 date times of consistently cold summers resulting in ice-cap expansion through the Common Era,
636 but are restricted to expansions for which subsequent summers never warmed sufficiently and/or
637 long enough to completely melt earlier ice-cap expansions. By inference, summers currently are
638 warmer than any series of multi-decadal summers since the dated ice-cap expansions, placing
639 contemporary warming in a millennial perspective. Kill-dates that define changes in ice cap
640 dimensions provide a reliable summer paleo-temperature proxy.

641

642 • None of the 107 kill-dates from plateau ice caps within the area inscribed in Fig. 1 pre-date the
643 Common Era. Consequently, if earlier Neoglacial episodes of summer cold resulted in long-lived ice
644 caps across the uplands, subsequent summers were warm enough and/or long enough to
645 completely melt those ice caps before 1 CE.

646

647 • The composite PDF of 186 moss Common-Era kill-dates collected from seventy ice caps over a
648 region covering more than 50,000 km² yields three multi-century clusters, defining times of
649 widespread ice-cap expansion 250-450 CE, 850-1000 CE, and 1240-1480 CE; ice margins continued
650 to expand after 1480 CE to a peak snowline lowering between 1780 and 1880 CE, resulting in over
651 ~11,000 km² covered by ice caps, across a region where ice caps currently cover <100 km².

652

653 • Intervals of ice-cap expansion defined by moss kill dates through the Common Era align
654 with centuries of persistent cold summers in the past2k fully coupled climate model for the
655 Common Era with all major forcings. The model simulates decadal averaged summer
656 temperatures that reveal a first-order decline in summer temperatures over the Common Era,
657 consistent with peak Neoglacial ice dimensions late in the Little Ice Age. Centennial intervals of cold

658 summers align with the clusters of kill-dates; warm modeled summers align with intervals lacking
659 kill dates. Peak Common Era modeled cold summers between 1780 and 1880 CE led to a snowline
660 decline that dramatically increased the snow-covered regions of the Baffin Island uplands
661 (Instantaneous Glacierization) and brought the Eastern Canadian Arctic perilously close to
662 conditions anticipated at the inception phase of the Laurentide Ice Sheet.

663

664 • Climate modeling over the interval from 1850 CE to present suggests that rapid ice-cap retreat
665 over Baffin Island beginning ~1880 CE, but especially after 1920 CE, was driven primarily by
666 anthropogenic forcing. We may never know with certainty whether the dramatic snowline decline,
667 and resultant aerial increase in permanently snow-covered lands in Arctic Canada at the peak of
668 the Little Ice Age heralded the onset of the next Northern Hemisphere ice age, only to be reversed
669 by the increase in greenhouse gases and other forcing agents related to the Industrial Revolution.
670 Summer insolation across the Arctic was near its orbitally driven minimum at the peak of the Little
671 Ice Age, and will continue to decrease slightly through the 21st Century. The strong positive
672 correlation between Arctic summer temperatures and summer insolation (Kaufman et al, 2009)
673 suggests that only the additional anthropogenic forcings since ~1850 CE reversed the natural
674 transition into a new ice age.

675

676 • Clusters of kill dates that define multi-decadal episodes of expanding Baffin Island Ice Caps align
677 with expanding margins of Langjökull, second largest ice cap in Iceland, as recorded in an annually
678 resolved continuous record through the Common Era from glacial lake Hvítárvatn. This correlation
679 suggests our record provides a North Atlantic Arctic template for Common Era summer
680 temperatures, with the coldest century of the Common Era occurring between 1780 and 1880 CE.

681

682

683 FIGURES

684



685

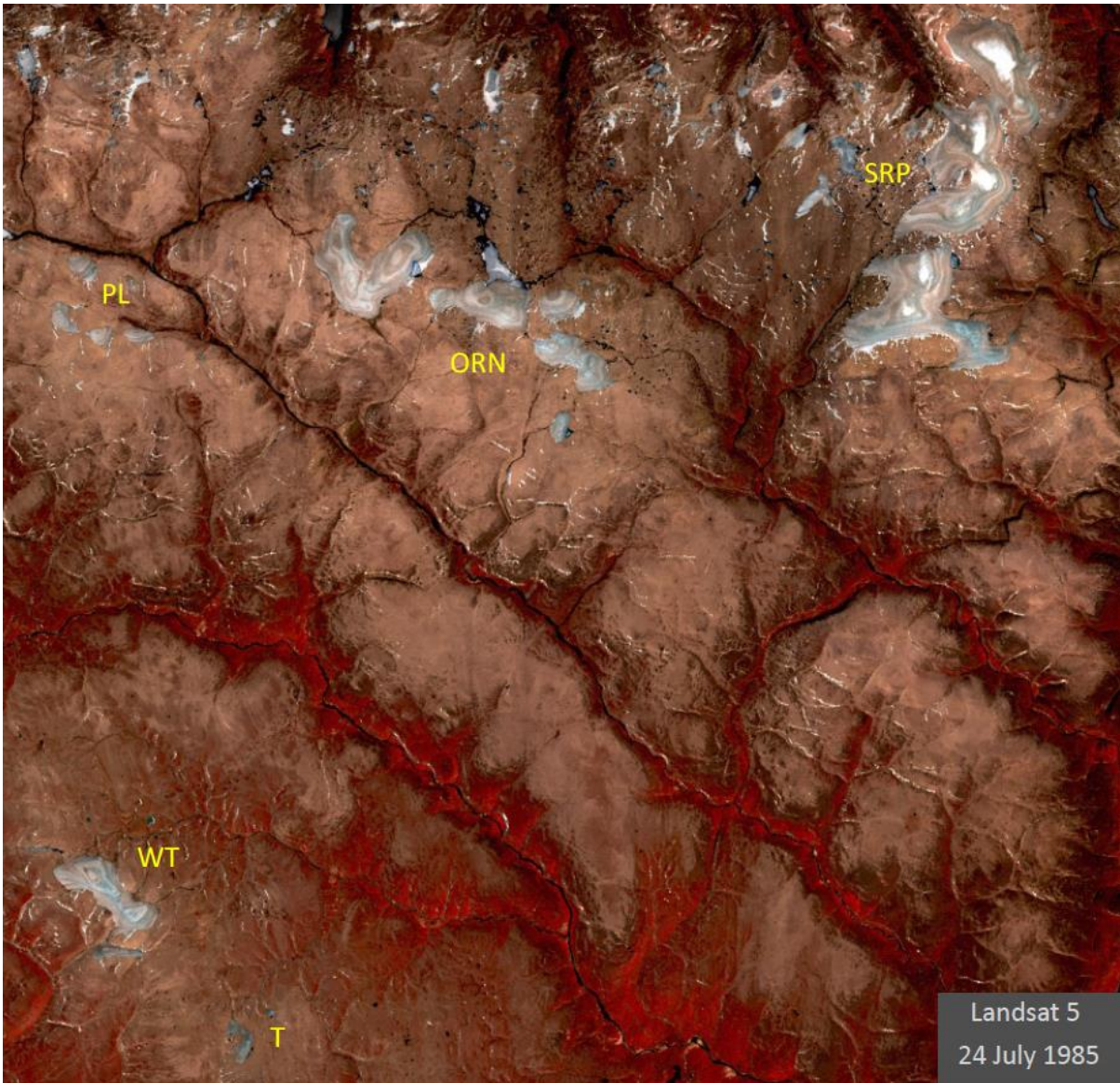
686

687 Figure 1 Field area, northern Baffin Island. Solid line defines regions for which the area-elevation
688 relation is quantified in Supplemental Figure 1 and used to reconstruct the area covered by
689 descending snowlines (Fig. 16), and the area of limited vegetation cover that defines ice-cap
690 outlines at the peak cold of the Little Ice Age. Dotted white square is the area covered by Fig. 2.
691 Encircled dots show locations of all 186 moss kill-dates (some dots include multiple samples). A
692 portion of the Barnes Ice Cap is in lower right corner. Inset upper right shows Baffin Island and
693 location of the basemap. Basemap © Google Earth.

694

695

696



697
698
699
700
701
702
703

704
705
706
707
708
709
710
711

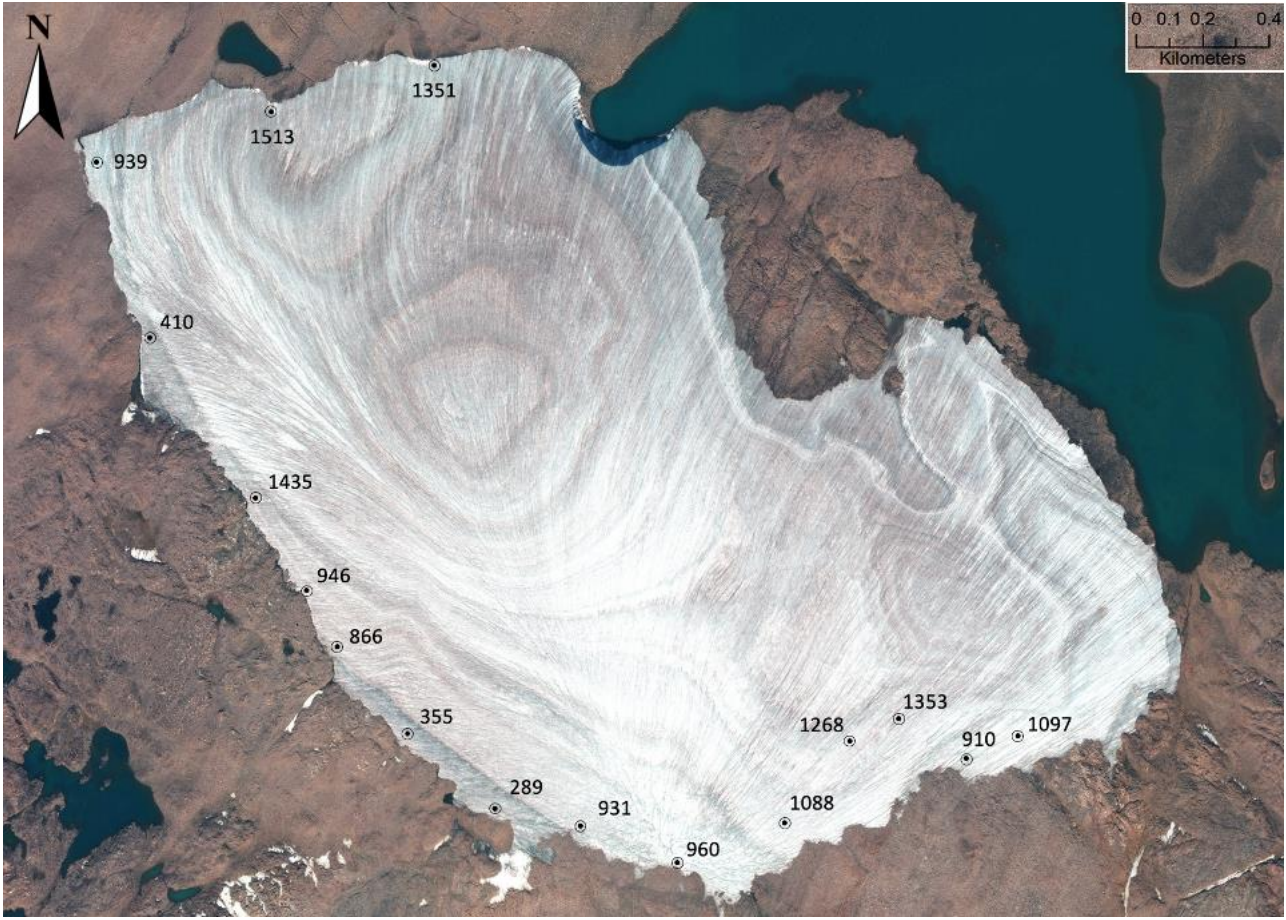
Figure 2. 1985 Landsat 5 image, color-enhanced to maximize the spectral contrast that highlights lighter-toned regions that are sparsely vegetated. Those regions were beneath ice caps for at least several decades during peak summer cold of the Little Ice Age. Labels are for the Serpens (SRP) and Orion (ORN) ice-cap complexes, White Tiger (WT) and Tiger (T) ice caps, and Pleiades ice-cap cluster (PL). Location of image shown in Figure 1.



712
713

714 Figure 3. Delicately perched boulder left by the receding Laurentide Ice Sheet that has recently
715 emerged by down-wasting of the local ice cap in background. Striae on the underlying bedrock are
716 toward the NE, the flow of regional Laurentide ice in this area at the LGM. The preservation of such
717 delicate features demonstrates the lack of internal deformation in cold-based ice caps that mantle
718 the low relief hills of the Baffin Island uplands. Photo by GHM.

719



720

721 Figure 4. Digital Globe image of one ice cap in the Orion Ice Complex (~4 km long axis) captured 20
 722 Aug. 2015, with median calibrated kill dates (CE year) for dead moss located at their ice-edge
 723 collection coordinates when collected in 2018. The three early CE kill dates (289, 355, 410 CE)
 724 are situated beneath ice with distinctive surface characteristics that differ from the rest of the ice cap,
 725 consistent with that being a remnant early CE ice cap that expanded, killing the moss, followed by
 726 partial retreat, and was then subsumed by a late First Millennium episode of ice-cap growth, as well
 727 as later Little Ice Age ice-cap growth, with dead moss now being revealed as ice is melting at all
 728 elevations. These small ice caps on nearly flat landscapes are frozen to their beds and exhibit little
 729 internal ice flow.

730

731

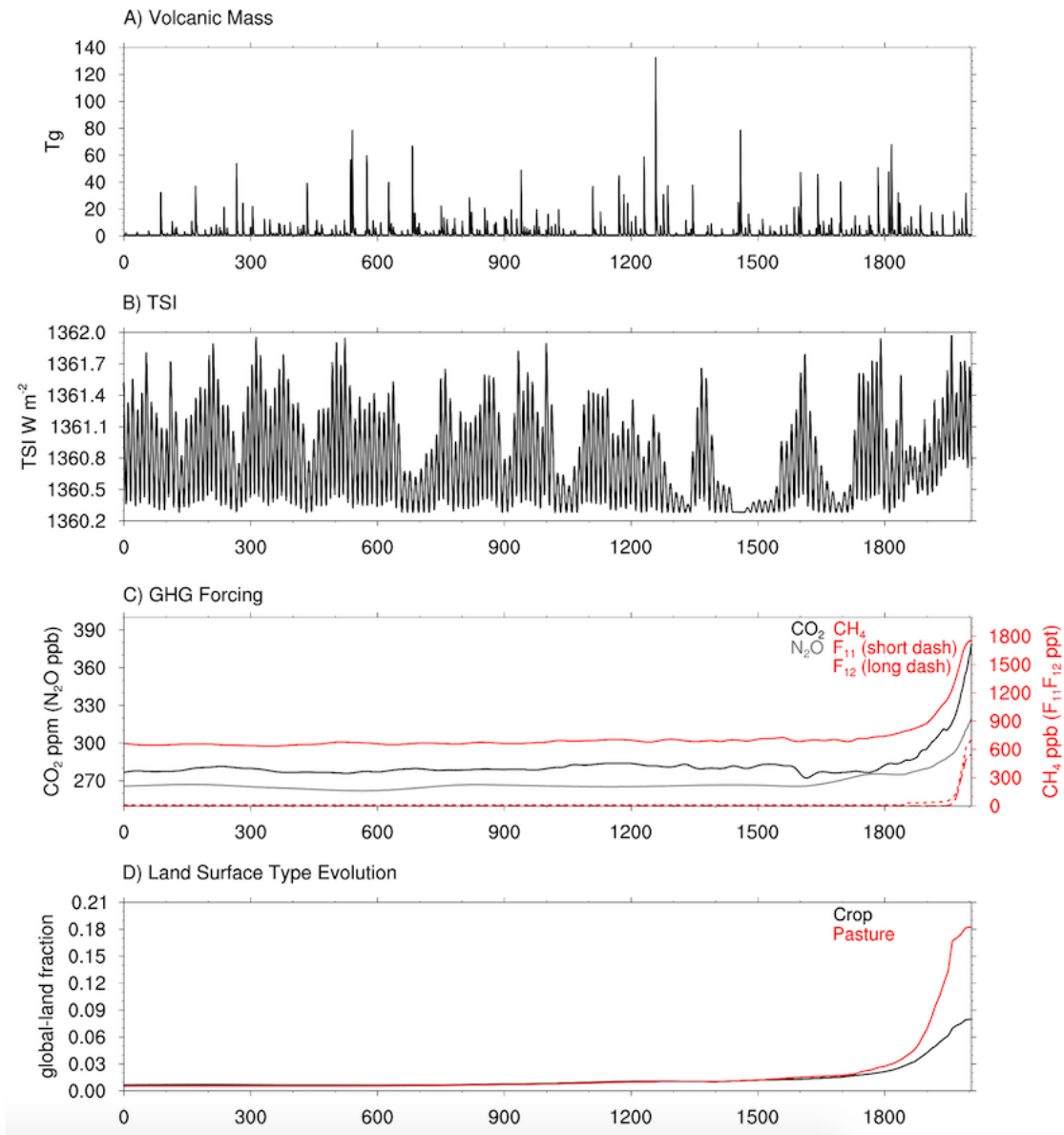
732

733

734

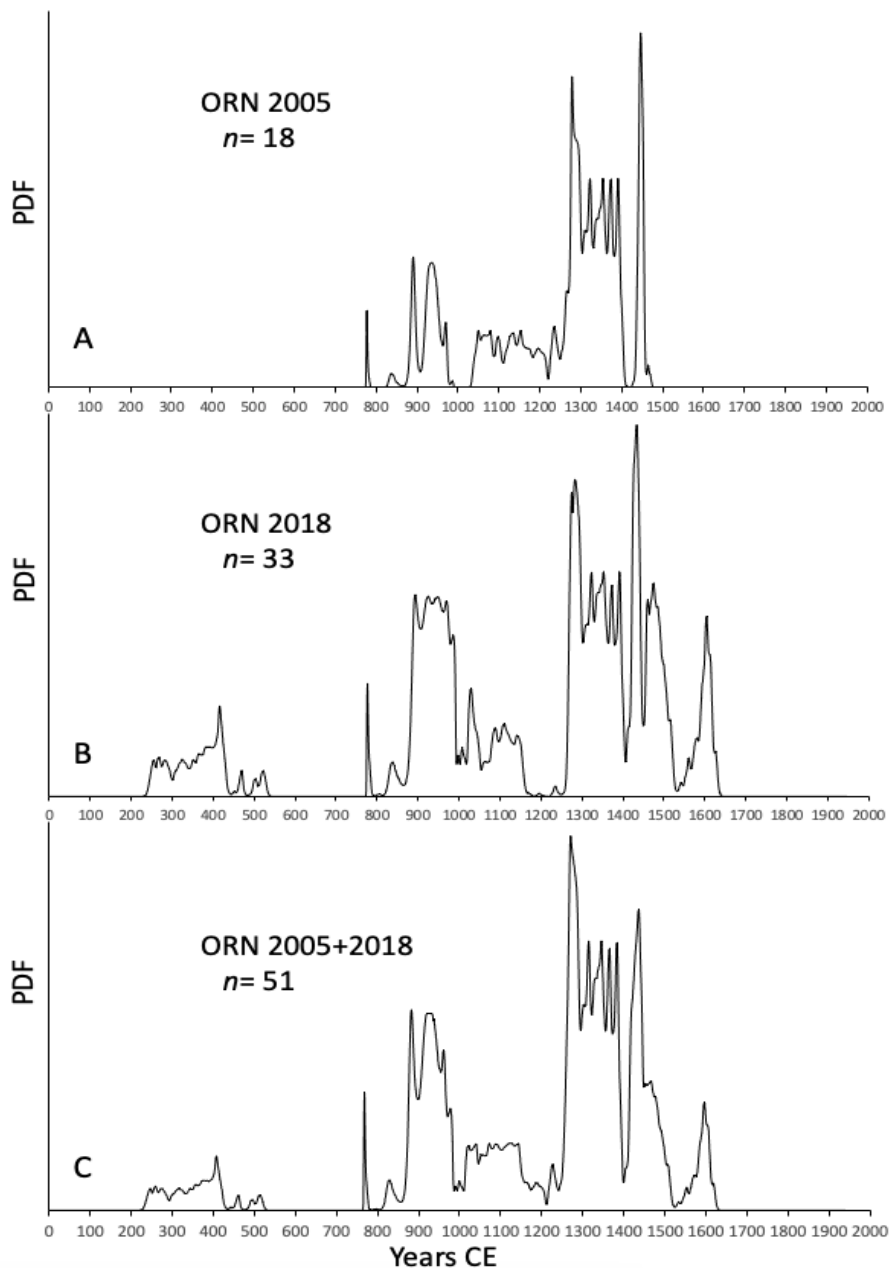
735

736



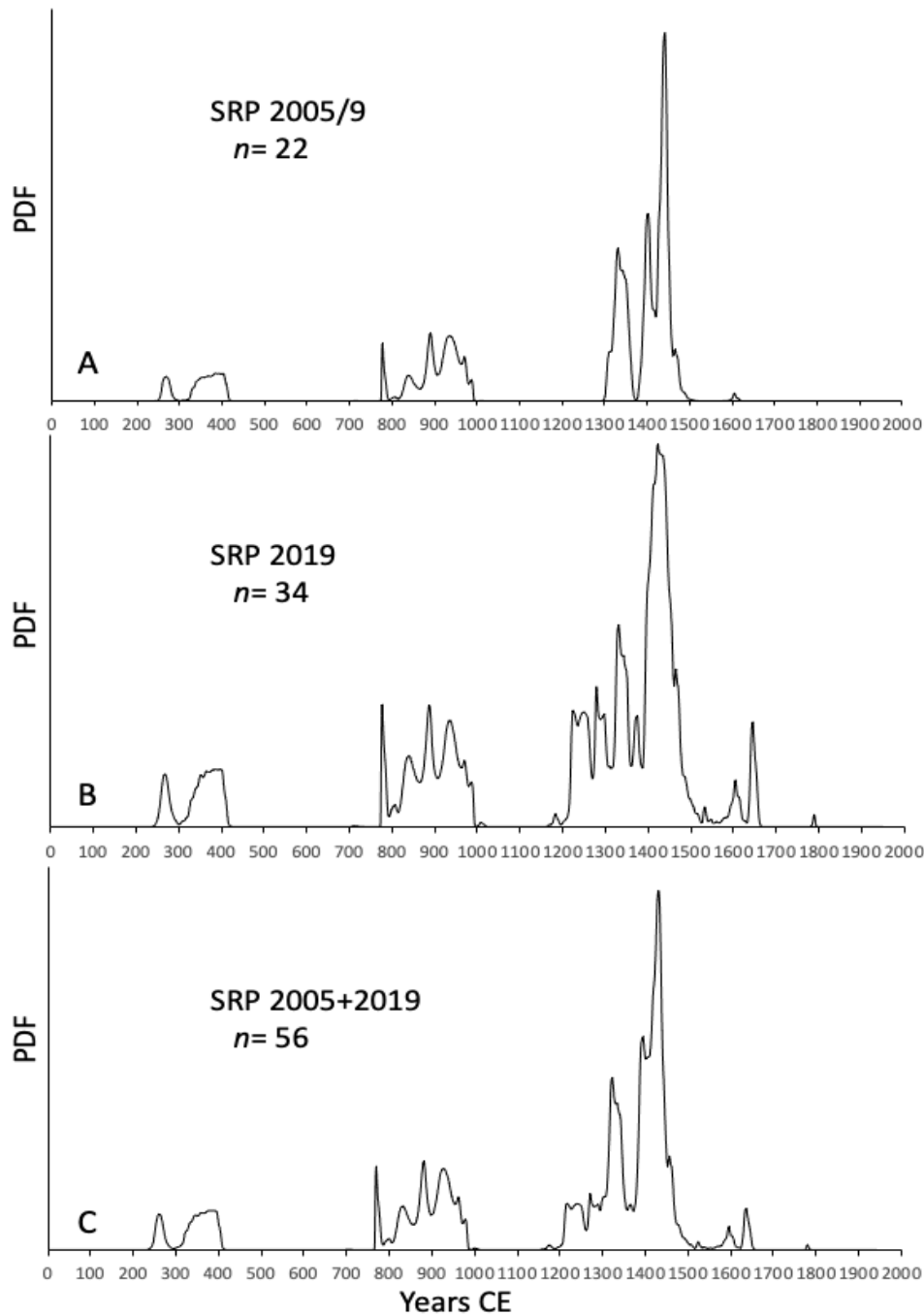
737
738

739 Figure 5. Forcing used for the past2k climate model discussed in the text. A) Mass of sulfuric acid
740 injected into the stratosphere by explosive volcanism in teragrams. B) Total solar irradiance (TSI) in
741 watts / m^2 . C) Concentrations of anthropogenic greenhouse gasses released through the Common
742 Era. D) Anthropogenic changes in global land cover through the development of crop (upper line)
743 and pasture (lower line) through the Common Era.



744
745
746
747
748
749
750
751
752

Figure 6 Probability density functions (PDF) for calibrated radiocarbon dates on dead moss collected around the margins of the Orion Ice Complex (ORN, Fig. 2), which consists of several adjacent ice caps. (A) The PDF of 18 samples collected in 2005. (B) The PDF of 33 samples collected in 2018, which mirror the distribution from 2005, except for the addition of early First Millennium samples in the latter group, that reflect a buried ice cap now emerging from beneath a younger ice cap that overwhelmed, but did not incorporate it (Fig. 4). (C) PDF of all dates from ORN from all years

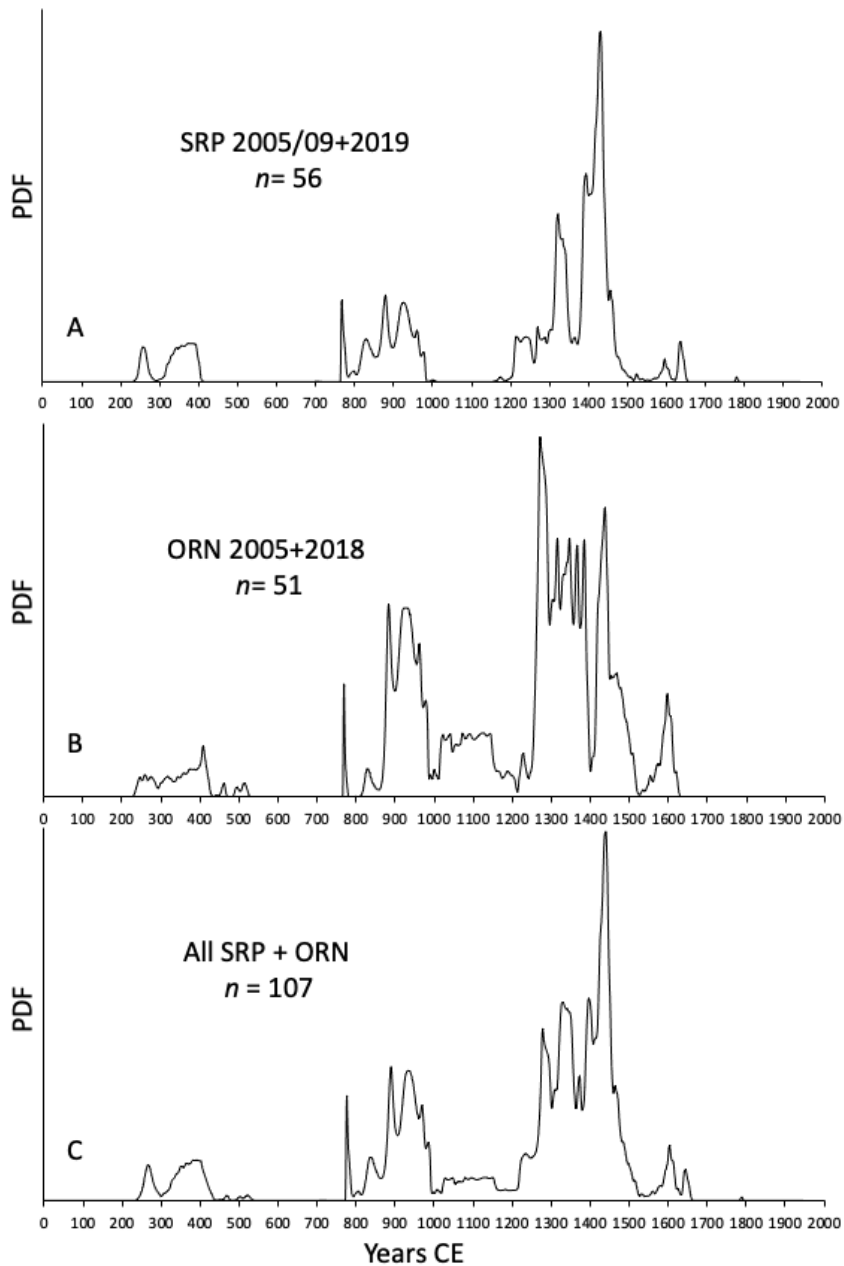


753 .

754

755

Figure 7. Probability density functions (PDF) for calibrated radiocarbon dates on dead moss collected around the margins of the Serpens Ice Complex (SRP, Fig. 2), which consists of three adjacent ice caps. (A) The PDF of 22 samples collected in 2005 and 3 others collected in 2009. (B) The PDF of 34 samples collected in 2019. (C) The composite PDF for all 56 kill dates from SRP form three discrete age clusters that exhibit little change between collection dates, despite significant (~250 m) ice-margin recession.



756

Figure 8. A comparison between probability density functions (PDF) for all calibrated radiocarbon dates on dead moss collected around the margins of ORN (A) and SRP (B) ice complexes (Fig. 2) showing the similarities between the two data sets. The composite PDF for the 107 moss kill-dates from both ice complexes (C) defines tightly clustered episodes of ice-cap expansion through the Common Era at 250-400 CE, 850-1000 CE, and between ~1240 and 1480 CE.

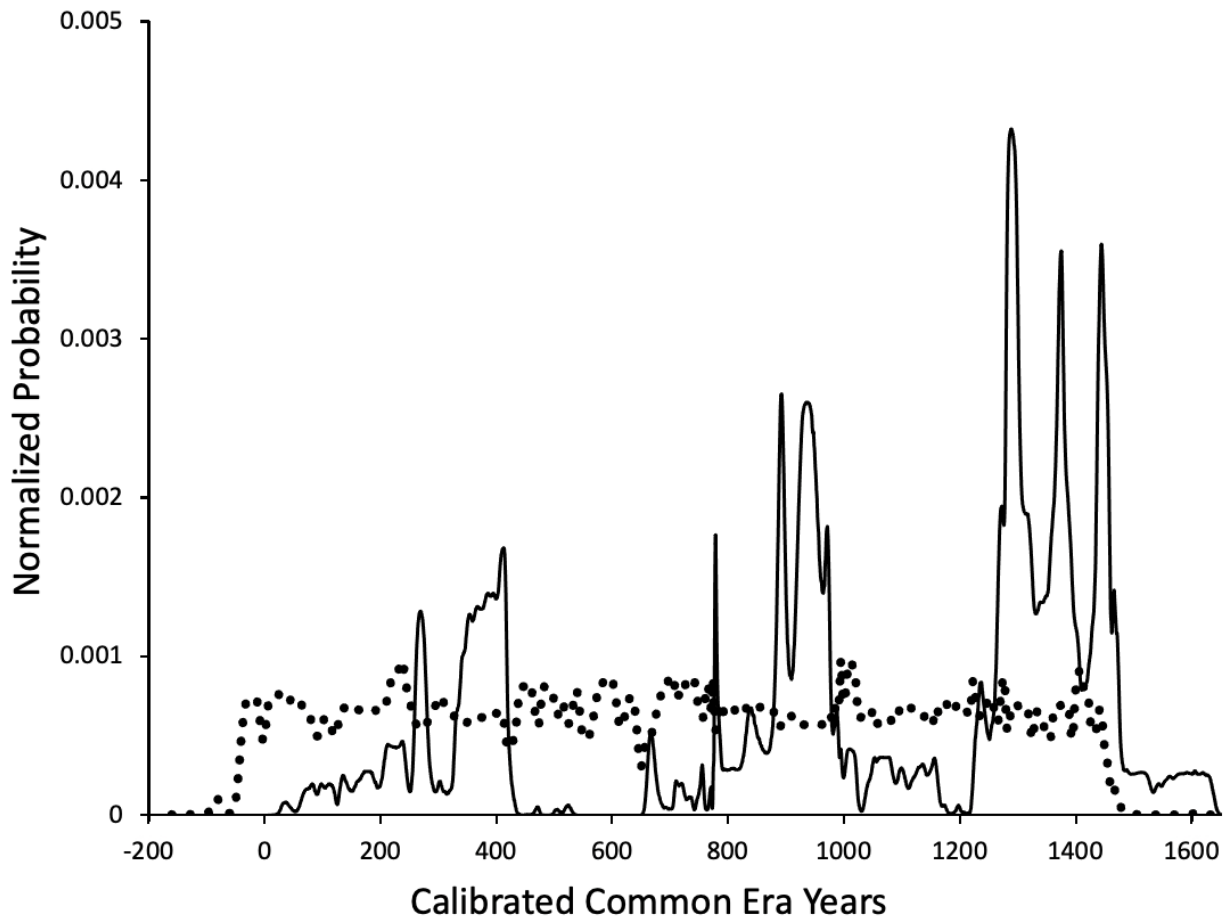
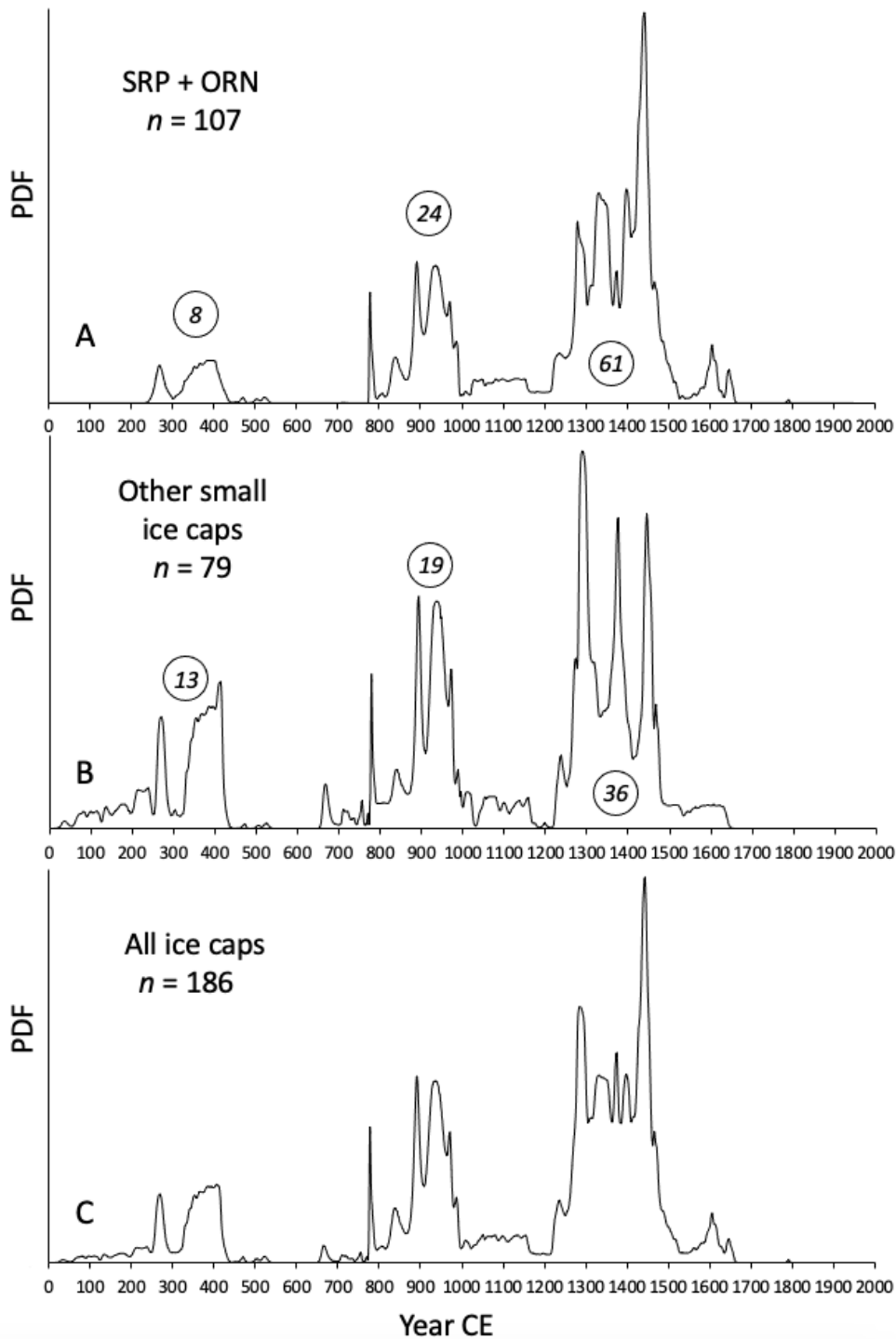


Figure 9 The composite PDF for calibrated ^{14}C ages of 186 calendar dates equally distributed between 1 and 1500 CE (dotted line) superposed on the same scale as the 186 calibrated “kill dates” to test whether changes in atmospheric $^{14}\text{CO}_2$ concentrations contributed to the clustering of kill dates in the SRP and ORN composite PDFs (Fig. 8). There is no strong correlation between the two PDFs, indicating any inherent calibration bias has no influence on the clustering of the moss kill dates.



760

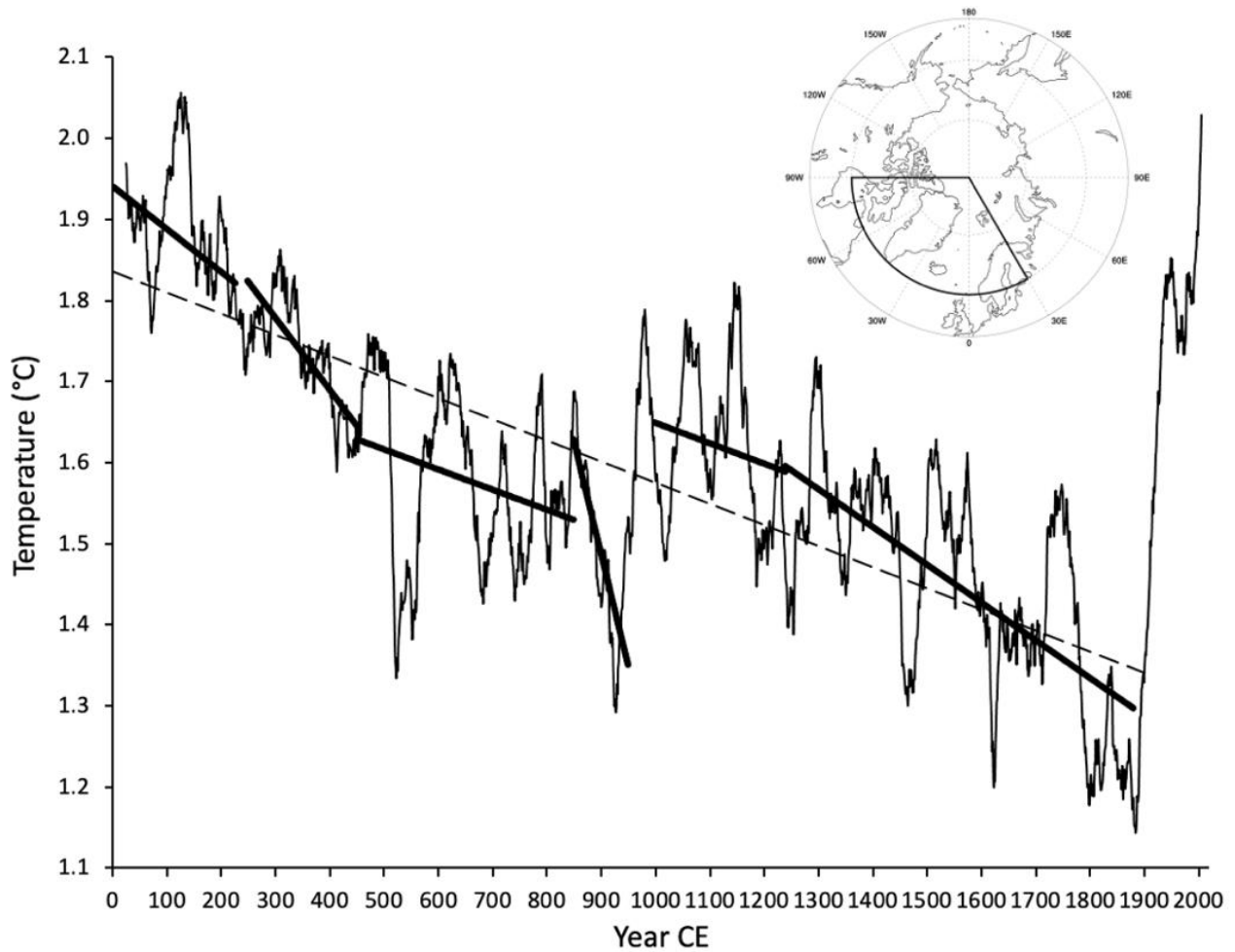
761

762 Figure 10. The PDF for all moss kill-dates from SRP+ORN (A) and from the margins of all other small ice caps in Fig. 1 (B)
 763 are composited in Panel C. Moss kill-dates that make up Panel B include all Common Era kill dates from 62 different ice caps
 764 caps (Fig. 1), all within 250 km of the SRP and ORN ice complexes. The number of dates in each of the clusters is given
 765 as a circled number. The similarities between PDFs in Panels A and B are striking, suggesting ice-cap response to climate
 766 forcing over the Common Era was uniform across northern Baffin Island, and lends confidence to a comparison of ice-
 767 cap response and modeled climate forcing. Location data, Lab-ID, ¹⁴C ages and the PDF for each sample in Panel C are
 768 available at the NSF Arctic Data Center (<https://arcticdata.io/catalog/view/doi:10.18739/A2RN30884>). The spike at
 769 ~780 CE is a calibration very low probability age in the calibration program.

770

771

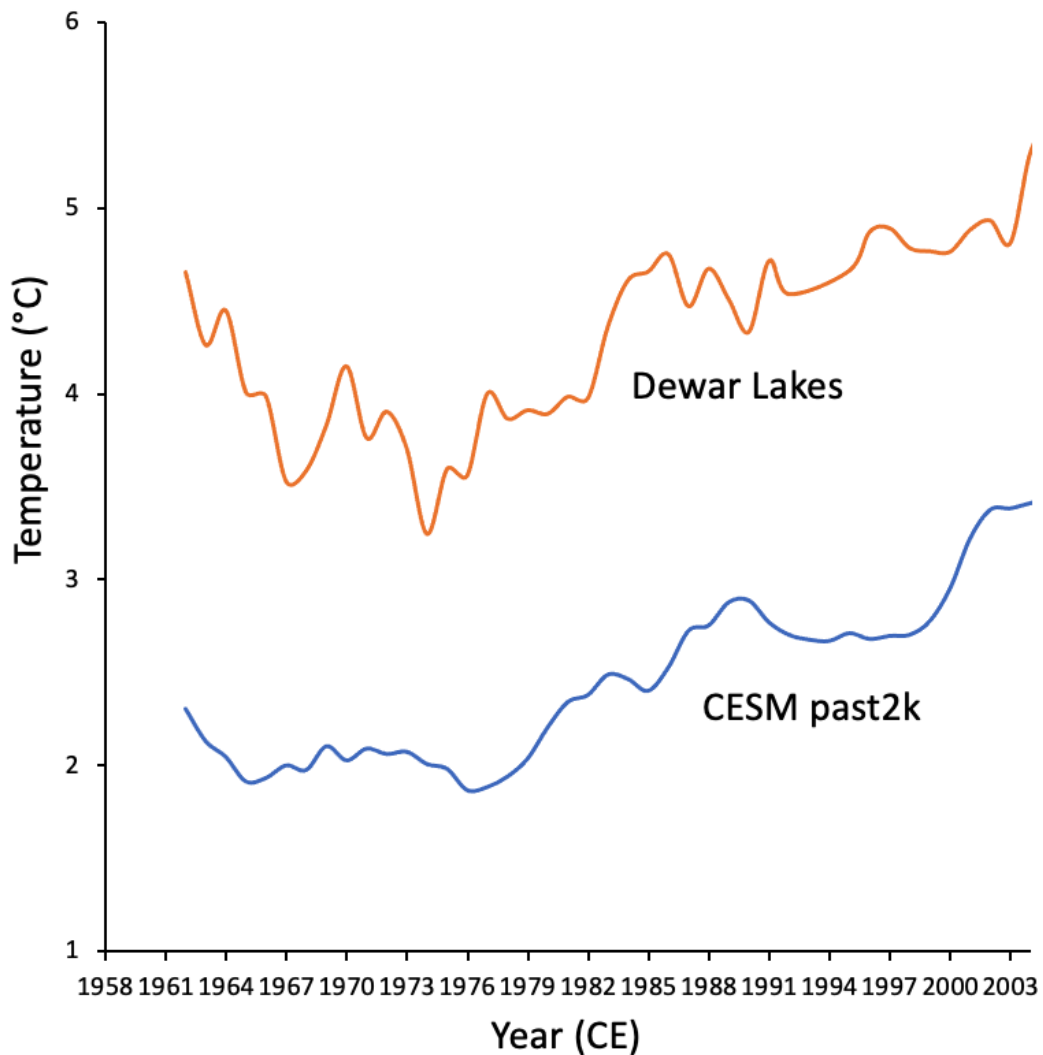
772



773

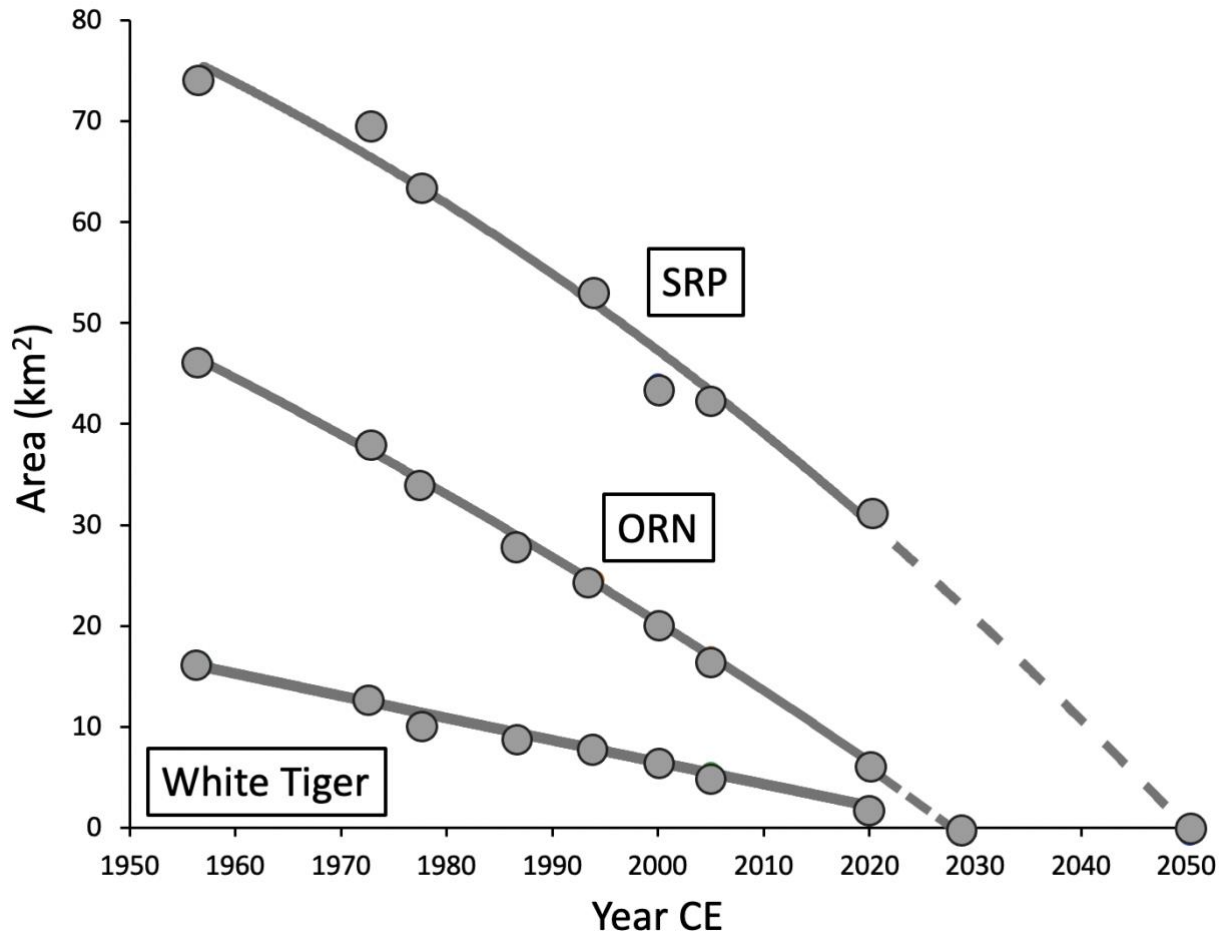
774

775 Figure 11 Fifty-year running mean of modeled annual summer (J, J, A) temperature over land areas north of
776 60° and between 30° and 90° west latitude (shown in inset) between years 1 and 2005 CE in our CESM past2k
777 simulation. Dashed black line is a least-squares linear regression for the data between 1 and 1890 CE,
778 showing a first order trend of declining summer temperature through the Common Era. Solid lines are least-
779 squares linear regressions through times defined by clusters of kill dates, and the times between kill-date
780 clusters in Figure 10C. The regressions allow a direct comparison of summer temperature trends and relative
781 magnitudes for intervals characterized by widespread ice-cap expansion (predicted cold summers), and
782 intervals lacking evidence of sustained ice-cap expansion (predicted mild summers). The time-intervals
783 defined by these trends can be compared to the reconstructed snowline elevations through the Common
784 Era (Fig. 16).



785
786
787
788
789
790
791
792
793
794
795
796
797
798
799
800

Figure 12 10-year running mean for JJA temperature measured daily at Dewar Lakes since 1958 (upper line) and 5-year running means of simulated JJA 2-m temperature over land north of 60°N and between 30°E and 90°W in our CESM past2k model run (lower line). Dewar Lakes temperatures are more strongly smoothed because site-specific records have greater variability than past2k, which is averaged over a large area that naturally smooths the data. The similarity in the patterns and magnitude of temperature change between model and data indicates that the past2k model reliably simulates the primary signal of summer temperatures across our field area through the Common Era.



801

802

803

804

805

806

807

808

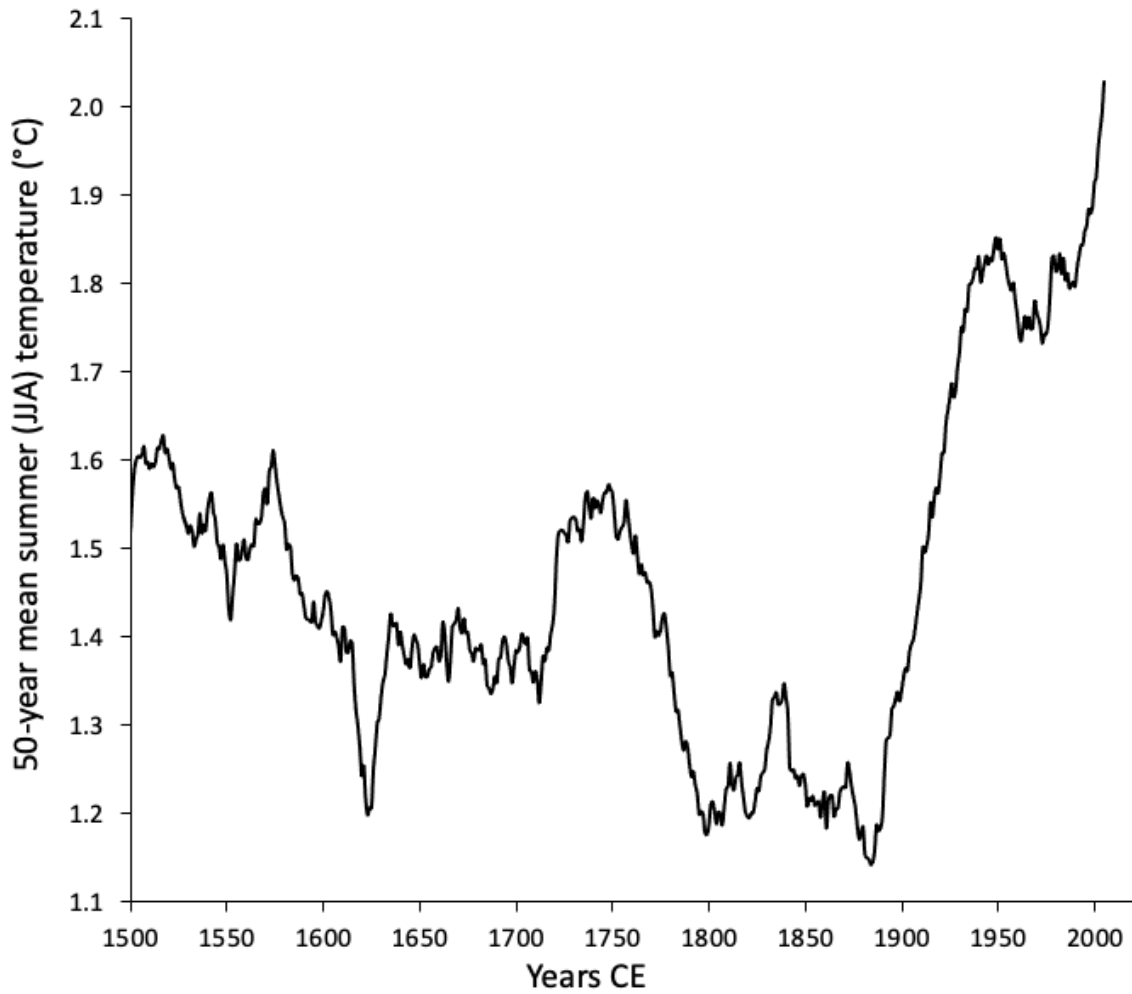
809

810

811

812

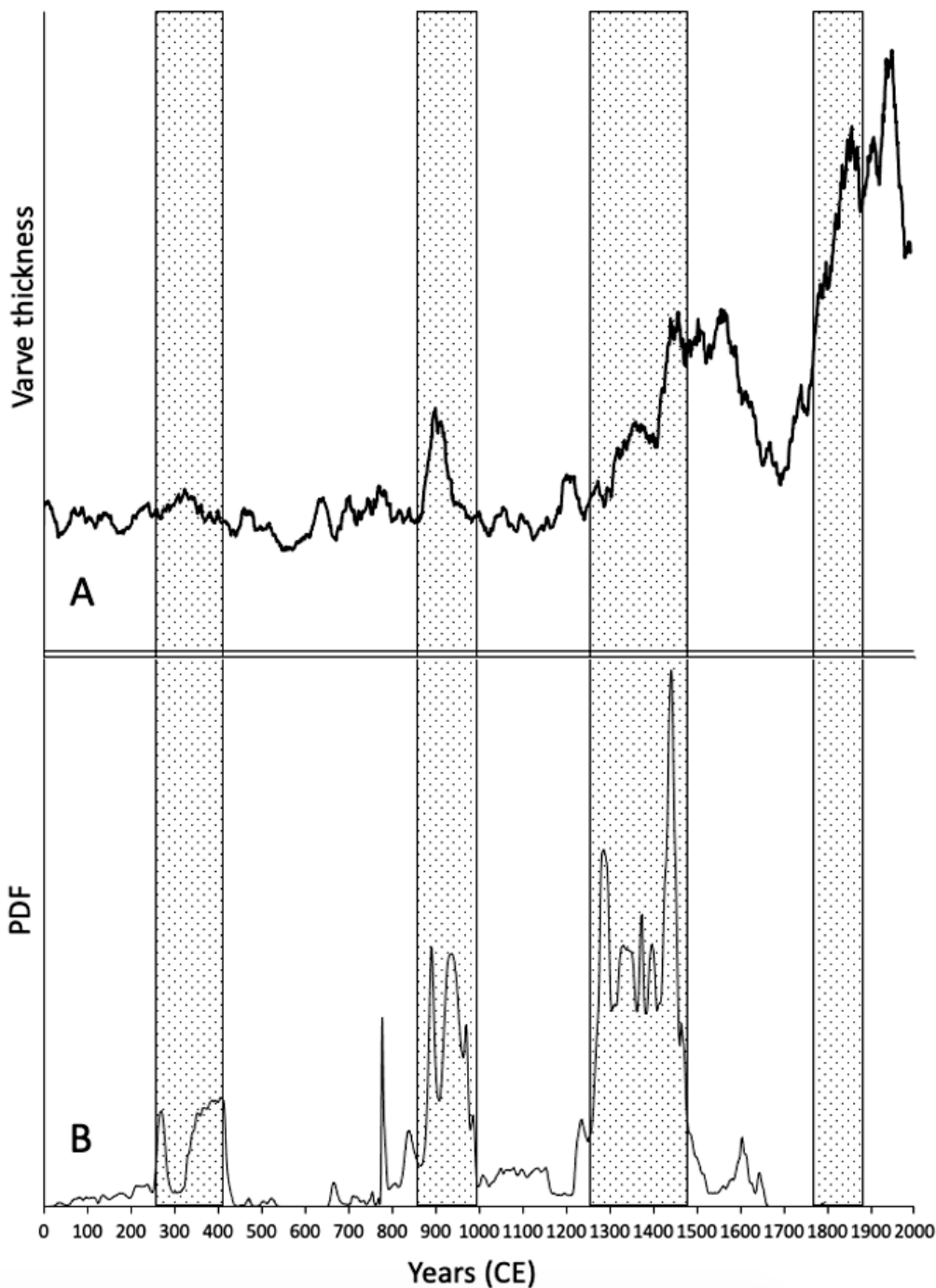
Figure 13 The change in area for three caps between 1957 and 2020 (Fig. 2); Serpens Ice Complex (SRP; 3 ice caps), Orion Ice Complex (ORN; 6 ice caps, 4 remaining in 2020 CE), and White Tiger (WT, one ice cap). All three show decreased recession rates between 1957 and 1972 CE, consistent with cold summers recorded at Dewar Lakes over the decade between 1958 and mid 1970s CE, followed by steady, or increasing rates of mass loss after 1972. Areas are derived from vertical aerial photography from 1957 CE and satellite imagery subsequently. Updated from Anderson et al. (2008).



813

814

Figure 14 Fifty-year running means of summer (JJA) temperatures in our past2k simulation illustrating the strong trend in declining summer temperatures after 1500 CE (our youngest kill dates), the peak cold century (1780-1880 CE) and rapid summer temperature rise after 1900 CE.



815

816

817

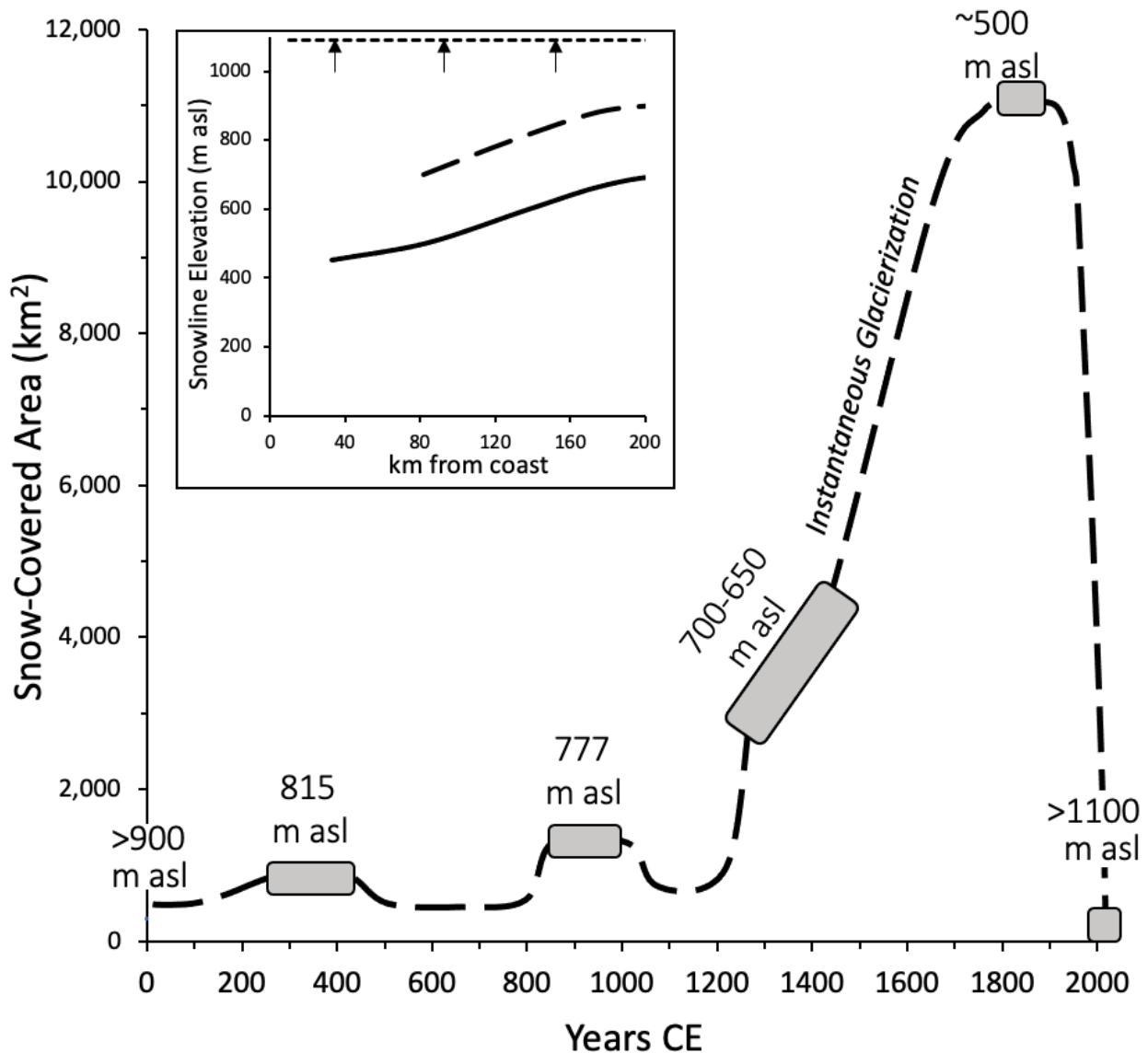
818

819

820

821

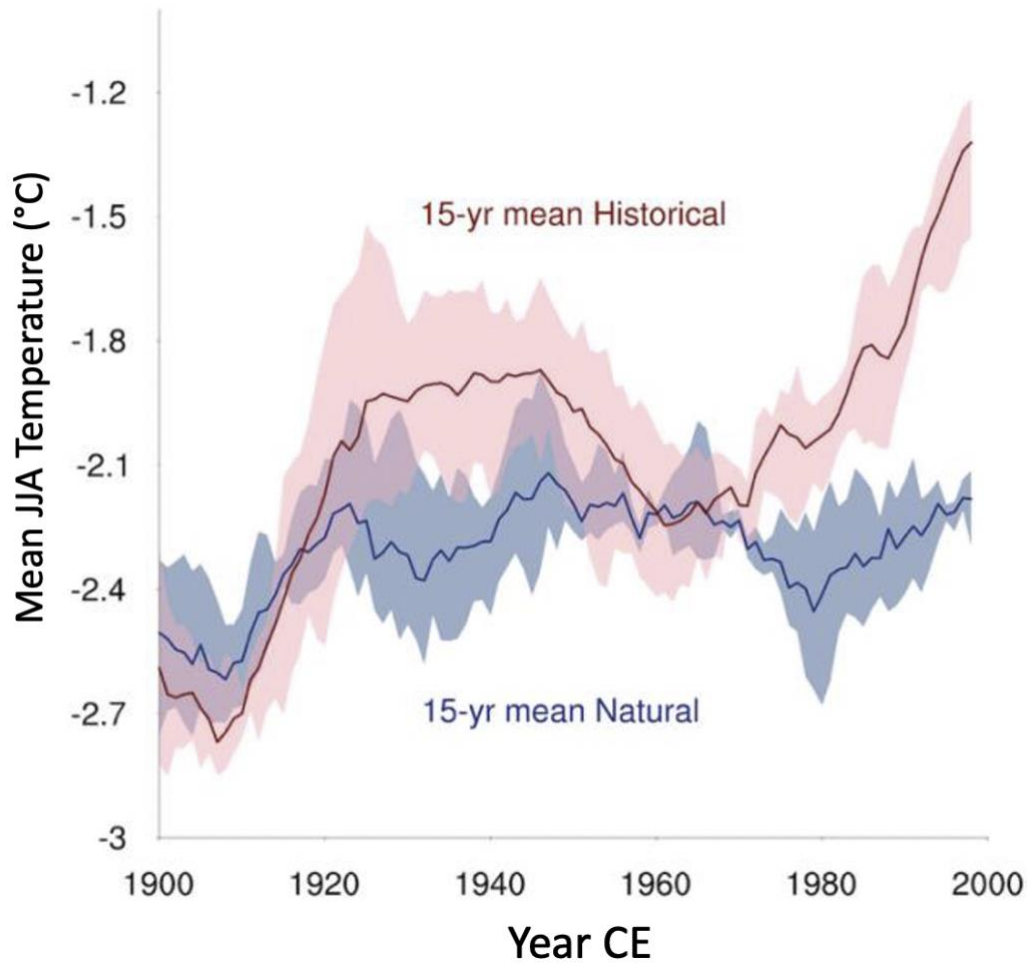
Figure 15 Comparison of 15-year running means of annual varve thickness in glacial lake Hvítárvatn (A), a proxy for the size of Langjökull, second largest glacier in Iceland, and 186 moss kill-dates from Baffin Island (B). Stippled boxes show the close correspondence between growth of Langjökull and expansion of Baffin Island ice caps. The varves also confirm that Langjökull attained its greatest dimension in the late 1800s CE, the same time Baffin Island snowline was at its lowest of the Common Era. The close correspondence of the two paleoclimate records suggest Baffin kill-dates and Hvítárvatn varves provide a broader North Atlantic Arctic temperature history for the Common Era.



822

823

Figure 16 Changes in ice-covered area through the Common Era within our prescribed field area (Fig. 1). Episodes of ice-cap expansion derived from moss kill-dates (Fig. 10C; square boxes) and their associated snowline elevation listed above each box, are plotted against the ice-covered area based on the area-elevation relation within the field area as shown in Supplemental Figure 3. The area covered by ice caps 1780-1880 CE is the summed areas defined by vegetation trim lines (Supplemental Figure 4), with the age derived from the past2k modeled temperatures (section 5.1). Inset shows the snowline elevations through our field area for 1880 CE (solid line), 1960 CE (dashed line) whereas snowline is currently everywhere above 2020 CE (dotted line). The dramatic increase in area of permanently covered ice as snowline descended through the Little Ice Age was originally postulated by Ives (1957) to result in “instantaneous glacierization” due to the significant albedo increase that might lead to the onset of an ice age (Andrews and Mahaffy, 1975; Clark et al., 1993; Birch et al., 2017).



824

825 Figure 17 Comparison of 15-year running means of summer (JJA) temperatures over Arctic lands
 826 north of 60°N, and between 30°E and 90°W for CESM-1 simulations initiated in 1850 CE with
 827 “Historical” forcings (natural + anthropogenic; 4 runs) and only “Natural” forcings (TSI, volcanism,
 828 insolation; 3 runs) for the 20th Century. Red and blue curves are ensemble means of the 4
 829 “Historical” runs and the 3 “Natural” runs respectively, with the ± 1 sigma ranges of the ensemble
 830 runs given by the shading. The early 20th Century rise in the “Historical” simulation is due primarily
 831 to GHG increases, with the subsequent decline primarily a result of additions of aerosols, which are
 832 reduced somewhat after 1960 as the continued increase in GHG dominates change. In contrast,
 833 there is no significant trend in the “Natural” simulations after 1920 CE.

834

835 **7. SUPPLEMENTAL DOCUMENTS**

836

837 **8. AUTHOR CONTRIBUTIONS**

838 GHM conceived the project. GHM, SLP, SJL, JPB, JHR, HB, MR collected samples, AJ and YZ were
839 responsible for climate modeling with assistance from ÁG and GHM. SJL and JRS were responsible
840 for the ¹⁴C dating. GHM wrote the manuscript with help from all authors.

841

842 **9. COMPETING INTERESTS:** The authors declare that they have no conflict of interest.

843

844 **10. ACKNOWLEDGEMENTS**

845 We gratefully acknowledge the Qikiqtaani Inuit and the Government of Nunavut for permission to
846 access their land through research permits issued by the Nunavut Research Institute. We thank the
847 Inuit of Qikiqtarjuaq for friendship, advice, and field guides over many decades, and members of
848 the Nunavut Research Institute for assistance in Iqaluit. Battelle ARO and Polar Continental Shelf
849 Program, Government of Canada, provided logistical support. We thank the INSTAAR Laboratory
850 for AMS Radiocarbon Preparation and Analysis for sample preparation, and The Keck Carbon Cycle
851 AMS Laboratory University of California, Irvine, for radiocarbon measurements. Digital Globe
852 acquired high-resolution imagery for some of our ice caps through a cooperative agreement with
853 the US-NSF. The field collections and dating were supported by the US National Science Foundation
854 through grants 0454662, 0909347, 1204096, 1418040, 1556627, and 1737715. Past2k climate
855 modeling was funded jointly by a Grant of Excellence (141573-053) from the Icelandic Research
856 Center (RANNIS) and the US National Science Foundation grant 1204096. The CESM project is
857 supported by the National Science Foundation and the Office of Science (BER) of the U.S.
858 Department of Energy. We acknowledge supercomputing resources for all used CESM simulations,
859 provided by NSF/CISL/Yellowstone and the Oak Ridge Leadership Computing Facility supported by
860 the Office of Science (BER) of the Department of Energy under Contract DE-AC05-00OR22725.

861 The past2k model output is available
862 at https://www.earthsystemgrid.org/dataset/ucar.cgd.cesm4.past2k_transient.html while the
863 natural forcing CESM simulations (b.e10.B2ONATC5CN.f09_g16) are available here
864 ([https://portal.nersc.gov/archive/home/c/ccsm/www/CESM-CAM5-SF-
865 No/atm/proc/tseries/monthly/TREFHT](https://portal.nersc.gov/archive/home/c/ccsm/www/CESM-CAM5-SF-No/atm/proc/tseries/monthly/TREFHT))

866 and the full forcing simulations (b.e10.B20TRC5CN.f09_g16) are available
867 at [https://www.earthsystemgrid.org/search.html?Project=CMIP5&q&page=1&rpp=20&Model=CE
868 SM1-CAM5&Experiment=historical](https://www.earthsystemgrid.org/search.html?Project=CMIP5&q&page=1&rpp=20&Model=CESM1-CAM5&Experiment=historical).

869 Dewar Lake climate data are available from [https://www.canada.ca/en/environment-climate-
870 change/](https://www.canada.ca/en/environment-climate-change/).

871 The 186 moss kill dates including their location and calibration are available at
872 <https://arcticdata.io/catalog/view/doi:10.18739/A2RN30884>.

873

874 11. REFERENCES

875 Literature Cited

- 876 Anderson, R.K., Miller, G.H., Briner, J.P., Lifton, N.A., DeVogel, S.B., 2008. A millennial perspective on Arctic warming
877 from ¹⁴C in quartz and plants emerging from beneath ice caps. 2008. *Geophysical Research Letters* 35 (1): L01502,
878 <https://doi.org/10.1029/2007GL032057>.
- 879 Andrews, J T; Davis, P T, Wright, C., 1976. Little Ice Age permanent snowcover in the Eastern Canadian Arctic: Extent
880 mapper from LandSat-1 satellite imagery. *Geog. Annaler*, 58A: 71-81.
- 881 Andrews, J T, and M A W Mahaffy. 1976. "Growth Rate of the Laurentide Ice Sheet and Sea Level Lowering (with
882 Emphasis on the 115,000 BP Sea Level Low)." *Quaternary Research* 6: 167–83.
- 883 Birch, Leah, Timothy Cronin, and Eli Tziperman. 2018. "The Role of Regional Feedbacks in Glacial Inception on Baffin
884 Island: The Interaction of Ice Flow and Meteorology." *Climate of the Past* 14 (10): 1441–62.
885 <https://doi.org/10.5194/cp-14-1441-2018>.
- 886 Birch, Leah, Timothy Cronin, and Eli Tziperman. 2017. "Glacial Inception on Baffin Island: The Role of Insolation,
887 Meteorology, and Topography." *Journal of Climate* 30 (11): 4047–64. <https://doi.org/10.1175/JCLI-D-16-0576.1>.
- 888 Briner, J P, P T Davis, and G H Miller. 2009. "Latest Pleistocene and Holocene Glaciation of Baffin Island, Arctic Canada:
889 Key Patterns and Chronologies." *Quaternary Science Reviews* 28: 2075–2087.
- 890 Briner, J.P., N. Michelutti, D.R. Francis, G.H. Miller, Y. Axford, M.J. Wooller, A.P. Wolfe, Y. Axford. and A.P. Wolfe. 2006.
891 "A Multi-Proxy Lacustrine Record of Holocene Climate Change on Northeastern Baffin Island, Arctic Canada."
892 *Quaternary Research* 65 (3): 431–42. <https://doi.org/10.1016/j.yqres.2005.10.005>.
- 893 Briner, Jason P., Nicholas P. McKay, Yarrow Axford, Ole Bennike, Raymond S. Bradley, Anne de Vernal, David Fisher, et
894 al. 2016. "Holocene Climate Change in Arctic Canada and Greenland." *Quaternary Science Reviews* 147: 340–64.
895 <https://doi.org/10.1016/j.quascirev.2016.02.010>.
- 896 Büntgen, Ulf, Vladimir S. Myglan, Fredrik Charpentier Ljungqvist, Michael McCormick, Nicola Di Cosmo, Michael Sigl,
897 Johann Jungclaus, et al. 2016. "Cooling and Societal Change during the Late Antique Little Ice Age from 536 to
898 around 660 AD." *Nature Geoscience* 9 (3): 231–36. <https://doi.org/10.1038/ngeo2652>.
- 899 Calkin, P. E., and J. M. Ellis. 1981. "A Cirque-Glacier Chronology Based on Emergent Lichens and Mosses." *Journal of*
900 *Glaciology* 27 (97): 511–15. <https://doi.org/10.1017/S0022143000011576>.
- 901 Clark, P. U., J. J. Clague, B. B. Curry, A. Dreimanis, S. R. Hicock, G. H. Miller, G. W. Berger, et al. 1993. "Initiation and
902 Development of the Laurentide and Cordilleran Ice Sheets Following the Last Interglaciation." *Quaternary Science*
903 *Reviews* 12 (2): 79–114. [https://doi.org/10.1016/0277-3791\(93\)90011-A](https://doi.org/10.1016/0277-3791(93)90011-A).
- 904 Clark, Peter U. 1994. "Unstable Behavior of the Laurentide Ice Sheet over Deforming Sediment and Its Implications for
905 Climate Change." *Quaternary Research*. <https://doi.org/10.1006/qres.1994.1002>.
- 906 Crump, S.E., L.S. Anderson, G.H. Miller, and R.S. Anderson. 2017. "Interpreting Exposure Ages from Ice-Cored Moraines:
907 A Neoglacial Case Study on Baffin Island, Arctic Canada." *Journal of Quaternary Science*.
908 <https://doi.org/10.1002/jqs.2979>.
- 909 Deser, Clara, Adam S. Phillips, Isla R. Simpson, Nan Rosenbloom, Dani Coleman, Flavio Lehner, Angeline G. Pendergrass,
910 Pedro Dinezio, and Samantha Stevenson. 2020. "Isolating the Evolving Contributions of Anthropogenic Aerosols

- 911 and Greenhouse Gases: A New CESM1 Large Ensemble Community Resource." *Journal of Climate* 33 (18): 7835–
912 58. <https://doi.org/10.1175/JCLI-D-20-0123.1>.
- 913 Dyke, Arthur S. 2004. "An Outline of North American Deglaciation with Emphasis on Central and Northern Canada."
914 *Developments in Quaternary Science 2 (PART B)*: 373–424. [https://doi.org/10.1016/S1571-0866\(04\)80209-4](https://doi.org/10.1016/S1571-0866(04)80209-4).
- 915 Francis, Jennifer A., Stephen J. Vavrus, and Judah Cohen. 2017. "Amplified Arctic Warming and Mid-Latitude Weather:
916 New Perspectives on Emerging Connections." *Wiley Interdisciplinary Reviews: Climate Change* 8 (5): 1–11.
917 <https://doi.org/10.1002/wcc.474>.
- 918 Fyfe, John C., Knut Von Salzen, Nathan P. Gillett, Vivek K. Arora, Gregory M. Flato, and Joseph R. McConnell. 2013. "One
919 Hundred Years of Arctic Surface Temperature Variation Due to Anthropogenic Influence." *Scientific Reports* 3: 1–
920 7. <https://doi.org/10.1038/srep02645>.
- 921 Gardner, A., G. Moholdt, A. Arendt, and B. Wouters. 2012. "Accelerated Contributions of Canada's Baffin and Bylot
922 Island Glaciers to Sea Level Rise over the Past Half Century." *Cryosphere* 6 (5): 1103–25.
923 <https://doi.org/10.5194/tc-6-1103-2012>.
- 924 Goldewijk, K., Beusen, A., Van Drecht, G. and De Vos, M., 2011. The HYDE 3.1 spatially explicit database of human-
925 induced global land-use change over the past 12,000 years. *Global Ecology and Biogeography*, 20(1), pp.73-
926 86. <https://doi.org/10.1111/j.1466-8238.2010.00587.x>
- 927 Groff, Dulcinea V., David W. Beilman, Zicheng Yu, Derek Ford, and Zhengyu Xia. 2023. "Kill Dates from Re-Exposed Black
928 Mosses Constrain Past Glacier Advances in the Northern Antarctic Peninsula." *Geology* 51 (3): 257–61.
929 <https://doi.org/10.1130/g50314.1>.
- 930 Harning, David J., Áslaug Geirsdóttir, Gifford H. Miller, and Leif Anderson. 2016. "Episodic Expansion of Drangajökull,
931 Vestfirðir, Iceland, over the Last 3 Ka Culminating in Its Maximum Dimension during the Little Ice Age."
932 *Quaternary Science Reviews* 152: 118–31. <https://doi.org/10.1016/j.quascirev.2016.10.001>.
- 933 Hugonnet, R., McNabb, R., Berthier, E. et al. Accelerated global glacier mass loss in the early twenty-first
934 century. *Nature* 592, 726–731 (2021). <https://doi.org/10.1038/s41586-021-03436-z>
- 935 Hurrell, James W., M. M. Holland, P. R. Gent, S. Ghan, Jennifer E. Kay, P. J. Kushner, J. F. Lamarque, et al. 2013. "The
936 Community Earth System Model: A Framework for Collaborative Research." *Bulletin of the American*
937 *Meteorological Society* 94 (9): 1339–60. <https://doi.org/10.1175/BAMS-D-12-00121.1>.
- 938 Ives, J D. 1957. Glaciation of the Torngat Mountains, Northern Labrador. *Arctic* 10: 67–87.
- 939 Ives, JD. 1962. Indications of recent extensive glacierization in north-central Baffin Island, NWT. *J. Glaciology* ,4: 197-
940 205 <https://doi.org/10.3189/S0022143000027398>
- 941 Ives, J D, J T Andrews, and R G Barry. 1975. "Growth and Decay of the Laurentide Ice Sheet and Comparisons with
942 Fenno-Scandinavia." *Die Naturwissenschaften* 62: 118–25.
- 943 Jungclaus, Johann H., Edouard Bard, Mélanie Baroni, Pascale Braconnot, Jian Cao, Louise P. Chini, Tania Egorova, et al.
944 2017. "The PMIP4 Contribution to CMIP6 - Part 3: The Last Millennium, Scientific Objective, and Experimental
945 Design for the PMIP4 Past1000 Simulations." *Geoscientific Model Development* 10 (11): 4005–33.
946 <https://doi.org/10.5194/gmd-10-4005-2017>.
- 947 Kleman, J, J Fastook, and A P Stroeven. 2002. "Geologically and Geomorphologically Constrained Numerical Model of
948 Laurentide Ice Sheet Inception and Build-Up." *Quaternary International* 95–6: 87–98.

- 949 Koerner, Roy M. 2005. "Mass Balance of Glaciers in the Queen Elizabeth Islands, Nunavut, Canada." *Annals of Glaciology*
950 42 : 417–23. <https://doi.org/10.3189/172756405781813122>.
- 951 Locke, C.W. and Locke, W.L.III. 1991. Little Ice Age Snow-Cover Extent and Paleoglaciation Thresholds: North-Central
952 Baffin Island, N.W.T., Canada *Arctic & Alpine Research* 23 (4): 436–43. <http://www.jstor.org/stable/1550544>.
- 953 Larsen, D.J., G.H. Miller, Á. Geirsdóttir, and T. Thordarson. 2011. "A 3000-Year Varved Record of Glacier Activity and
954 Climate Change from the Proglacial Lake Hvítárvatn, Iceland." *Quaternary Science Reviews* 30 (19–20).
955 <https://doi.org/10.1016/j.quascirev.2011.05.026>.
- 956 Lecavalier, Benoit S., David A. Fisher, Glenn A. Milne, Bo M. Vinther, Lev Tarasov, Philippe Huybrechts, Denis Lacelle, et
957 al. 2017. "High Arctic Holocene Temperature Record from the Agassiz Ice Cap and Greenland Ice Sheet Evolution."
958 *Proceedings of the National Academy of Sciences of the United States of America* 114 (23): 5952–57.
959 <https://doi.org/10.1073/pnas.1616287114>.
- 960 Lenaerts, Jan T.M., Jan H. Van Angelen, Michiel R. Van Den Broeke, Alex S. Gardner, Bert Wouters, and Erik Van
961 Meijgaard. 2013. "Irreversible Mass Loss of Canadian Arctic Archipelago Glaciers." *Geophysical Research Letters*
962 40 (5): 870–74. <https://doi.org/10.1002/grl.50214>.
- 963 Lowell, Thomas V., Brenda L. Hall, Meredith A. Kelly, Ole Bennike, Amanda R. Lusas, William Honsaker, Colby A. Smith,
964 Laura B. Levy, Scott Travis, and George H. Denton. 2013. "Late Holocene Expansion of Istorvet Ice Cap, Liverpool
965 Land, East Greenland." *Quaternary Science Reviews* 63: 128–40.
966 <https://doi.org/10.1016/j.quascirev.2012.11.012>.
- 967 MacFarling Meure, C., D. Etheridge, C. Trudinger, P. Steele, R. Langenfelds, T. Van Ommen, A. Smith, and J. Elkins. 2006.
968 "Law Dome CO₂, CH₄ and N₂O Ice Core Records Extended to 2000 Years BP." *Geophysical Research Letters* 33
969 (14): 2000–2003. <https://doi.org/10.1029/2006GL026152>.
- 970 Margreth, A., Dyke, A.S., Gosse, J.C., Telka, A.M. 2014. "Neoglacial Ice Expansion and Late Holocene Cold-Based Ice Cap
971 Dynamics on Cumberland Peninsula, Baffin Island, Arctic Canada." *Quaternary Science Reviews* 91: 242–56.
972 <https://doi.org/10.1016/j.quascirev.2014.02.005>.
- 973 Medford, Aaron K., Brenda L. Hall, Thomas V. Lowell, Meredith A. Kelly, Laura B. Levy, Paul S. Wilcox, and Yarrow Axford.
974 2021. "Holocene Glacial History of Renland Ice Cap, East Greenland, Reconstructed from Lake Sediments."
975 *Quaternary Science Reviews* 258: 106883. <https://doi.org/10.1016/j.quascirev.2021.106883>.
- 976 Medrzycka, Dorota, Luke Copland, and Brice Noël. 2023. "Rapid Demise and Committed Loss of Bowman Glacier,
977 Northern Ellesmere Island, Arctic Canada." *Journal of Glaciology*, 1–14. <https://doi.org/10.1017/jog.2022.119>.
- 978 Meehl, G.A., A. Hu, F. Castruccio, M.H. England, S.C. Bates, G. Donabasoglu, S. McGregor, J.M. Arblaster, S.-P. Xie, and
979 N. Rosenbloom, 2020: Atlantic and Pacific tropics connected by mutually interactive decadal-timescale
980 processes, *Nature Geo.*, doi:10.1038/s41561-020-00669-x.
- 981 Miller, G.H. 1973. Late Quaternary Glacial and Climatic History of Northern Cumberland Peninsula, Baffin Island, N.W.T.,
982 Canada. *Quaternary Research* 3: 561-583
- 983 Miller, G H, A Geirsdottir, Y Zhong, D J Larsen, B Otto-Bliesner, M M Holland, D A Bailey, et al. 2012. "Abrupt Onset of
984 the Little Ice Age Triggered by Volcanism and Sustained by Sea-Ice/Ocean Feedbacks." *Geophysical Research*
985 *Letters* 39. <https://doi.org/10.1029/2011GL050168>.
- 986 Miller, G.H., R.B. Alley, J. Brigham-Grette, J.J. Fitzpatrick, L. Polyak, M.C. Serreze, and J.W.C. White. 2010. "Arctic
987 Amplification: Can the Past Constrain the Future?" *Quaternary Science Reviews* 29 (15–16): 1779–90.
988 <https://doi.org/10.1016/j.quascirev.2010.02.008>.

- 989 Miller, G.H., A.P. Wolfe, J.P. Briner, P.E. Sauer, and A. Nesje. 2005. "Holocene Glaciation and Climate Evolution of Baffin
990 Island, Arctic Canada." *Quaternary Science Reviews* 24 (14–15): 1703–21.
991 <https://doi.org/10.1016/j.quascirev.2004.06.021>.
- 992 Miller, G.H., J.Y. Landvik, S.J. Lehman, and J.R. Southon. 2017. "Episodic Neoglacial Snowline Descent and Glacier
993 Expansion on Svalbard Reconstructed from the ¹⁴C Ages of Ice-Entombed Plants." *Quaternary Science Reviews*
994 155. <https://doi.org/10.1016/j.quascirev.2016.10.023>.
- 995 Miller, Gifford H., Scott J. Lehman, Kurt A. Refsnider, John R. Southon, and Yafang Zhong. 2013. "Unprecedented Recent
996 Summer Warmth in Arctic Canada." *Geophysical Research Letters* 40 (21): 5745–51.
997 <https://doi.org/10.1002/2013GL057188>.
- 998 Moore, J.J., K A Kughen, G.H. Miller, J.T. Overpeck. 2001. Little Ice Age Recorded in Summer Temperature
999 Reconstruction from Varved Sediments of Donard Lake, Baffin Island, Canada. *Journal of Paleolimnology* 25 (4):
1000 503–17. <https://doi.org/10.1023/A:1011181301514>.
- 1001 Myhre, G., B. H. Samset, M. Schulz, Y. Balkanski, S. Bauer, T. K. Berntsen, H. Bian, et al. 2013. Radiative Forcing of the
1002 Direct Aerosol Effect from AeroCom Phase II Simulations. *Atmospheric Chemistry and Physics* 13 (4): 1853–77.
1003 <https://doi.org/10.5194/acp-13-1853-2013>.
- 1004 Noël, Brice, Willem Jan van de Berg, Stef Lhermitte, Bert Wouters, Nicole Schaffer, and Michiel R. van den Broeke. 2018.
1005 "Six Decades of Glacial Mass Loss in the Canadian Arctic Archipelago." *Journal of Geophysical Research: Earth*
1006 *Surface* 123 (6): 1430–49. <https://doi.org/10.1029/2017JF004304>.
- 1007 Otto-Bliesner, Bette L., Esther C. Brady, John Fasullo, Alexandra Jahn, Laura Landrum, Samantha Stevenson, Nan
1008 Rosenbloom, Andrew Mai, and Gary Strand. 2016. Climate Variability and Change since 850 Ce an Ensemble
1009 Approach with the Community Earth System Model. *Bulletin of the American Meteorological Society* 97 (5): 787–
1010 801. <https://doi.org/10.1175/BAMS-D-14-00233.1>.
- 1011 Pendleton, S.L., G.H. Miller, R.A. Anderson, S.E. Crump, Y. Zhong, A. Jahn, and Á. Geirsdottir. 2017. "Episodic Neoglacial
1012 Expansion and Rapid 20th Century Retreat of a Small Ice Cap on Baffin Island, Arctic Canada, and Modeled
1013 Temperature Change." *Climate of the Past* 13 (11). <https://doi.org/10.5194/cp-13-1527-2017>.
- 1014 Pendleton, Simon L., Gifford H. Miller, Nathaniel Lifton, Scott J. Lehman, John Southon, Sarah E. Crump, and Robert S.
1015 Anderson. 2019. Rapidly Receding Arctic Canada Glaciers Revealing Landscapes Continuously Ice-Covered for
1016 More than 40,000 Years. *Nature Communications* 10 (1): 1–8. <https://doi.org/10.1038/s41467-019-08307-w>.
- 1017 Pendleton, Simon, Gifford Miller, Nathaniel Lifton, and Nicolás Young. 2019. Cryosphere Response Resolves Conflicting
1018 Evidence for the Timing of Peak Holocene Warmth on Baffin Island, Arctic Canada." *Quaternary Science Reviews*
1019 216: 107–15. <https://doi.org/10.1016/j.quascirev.2019.05.015>.
- 1020 Ramsey, Christopher Bronk, Richard A. Staff, Charlotte L. Bryant, Fiona Brock, Hiroyuki Kitagawa, Johannes Van Der
1021 Plicht, Gordon Scholou, et al. 2012. "A Complete Terrestrial Radiocarbon Record for 11.2 to 52.8 Kyr B.P." *Science*
1022 338 (6105): 370–74. <https://doi.org/10.1126/science.1226660>.
- 1023 Rantanen M, Karpechko AY, Lipponen A, Nordling K, Hyvärinen O, Ruosteenoja K, Vihma T, Laaksonen A. 2022. The
1024 Arctic has warmed nearly four times faster than the globe since 1979. *Communications Earth & Environment* 3:
1025 168.
- 1026 Reimer, Paula J., William E.N. Austin, Edouard Bard, Alex Bayliss, Paul G. Blackwell, Christopher Bronk Ramsey, Martin
1027 Butzin, et al. 2020. "The IntCal20 Northern Hemisphere Radiocarbon Age Calibration Curve (0-55 Cal KBP)." *Radiocarbon* 62 (4): 725–57. <https://doi.org/10.1017/RDC.2020.41>.

- 1029 Schweinsberg, A.D., J.P. Briner, G.H. Miller, O. Bennike, and E.K. Thomas. 2017. "Local Glaciation in West Greenland
1030 Linked to North Atlantic Ocean Circulation during the Holocene." *Geology* 45 (3).
1031 <https://doi.org/10.1130/G38114.1>.
- 1032 Schweinsberg, Avriel D, Jason P Briner, Gifford H Miller, Nathaniel A Lifton, Ole Bennike, and Brandon L Graham. 2018.
1033 "Holocene Mountain Glacier History in the Sukkertoppen Iskappe Area , Southwest Greenland." *Quaternary*
1034 *Science Reviews* 197: 142–61. <https://doi.org/10.1016/j.quascirev.2018.06.014>.
- 1035 Serreze, M. C., A. P. Barrett, J. C. Stroeve, D. N. Kindig, and M. M. Holland. 2009. "The Emergence of Surface-Based
1036 Arctic Amplification." *Cryosphere* 3 (1): 11–19. <https://doi.org/10.5194/tc-3-11-2009>.
- 1037 Sigl, M. et al. 2015. Timing and climate forcing of volcanic eruptions for the past 2,500 years. *Nature* 523, 543–549.
1038
- 1039 Søndergaard, Anne Sofie, Nicolaj Krog Larsen, Jesper Olsen, Astrid Strunk, and Sarah Woodroffe. 2019. "Glacial History
1040 of the Greenland Ice Sheet and a Local Ice Cap in Qaanaaq, Northwest Greenland." *Journal of Quaternary Science*
1041 34 (7): 536–47. <https://doi.org/10.1002/jqs.3139>.
- 1042 Taylor, K. E., R. J. Stouffer, and G. A. Meehl, 2012: An Overview of CMIP5 and the Experiment Design. *Bull. Amer.*
1043 *Meteor. Soc.*, 93, 485–498, <https://doi.org/10.1175/BAMS-D-11-00094.1>. Tepes, P., Gourmelen, N., Nienow, P.,
1044 Tsamados, M., Shepherd, A. and Weissgerber, F., 2021. Changes in elevation and mass of Arctic glaciers and ice
1045 caps, 2010–2017. *Remote Sensing of Environment*, 261, p.112481. <https://doi.org/10.1016/j.rse.2021.112481>
- 1046 Werner, Johannes P., Dmitry V. Divine, Fredrik Charpentier Ljungqvist, Tine Nilsen, and Pierre Francus. 2018. "Spatio-
1047 Temporal Variability of Arctic Summer Temperatures over the Past 2 Millennia." *Climate of the Past* 14 (4): 527–
1048 57. <https://doi.org/10.5194/cp-14-527-2018>.
- 1049 Williams, L. D. 1978. "The Little Ice Age Glaciation Level on Baffin Island, Arctic Canada." *Palaeogeography,*
1050 *Palaeoclimatology, Palaeoecology* 25 (3): 199–207. [https://doi.org/10.1016/0031-0182\(78\)90036-6](https://doi.org/10.1016/0031-0182(78)90036-6).
- 1051 Wolken, Gabriel J., John H. England, and Arthur S. Dyke. 2005. "Re-Evaluating the Relevance of Vegetation Trimlines in
1052 the Canadian Arctic as an Indicator of Little Ice Age Paleoenvironments." *Arctic* 58 (4): 341–53.
1053 <https://doi.org/10.14430/arctic448>.
- 1054 Xu, Y., Lin, L., Diao, C., Wang, Z., Bates, S., & Arblaster, J. (2022). The response of precipitation extremes to the
1055 twentieth- and twenty-first-century global temperature change in a comprehensive suite of CESM1 large
1056 ensemble simulation: Revisiting the role of forcing agents vs. the role of forcing magnitudes. *Earth and Space*
1057 *Science*, 9, e2021EA002010. <https://doi.org/10.1029/2021EA002010>
- 1058 Zhao, Alcide, David S. Stevenson, and Massimo A. Bollasina. 2019. "Climate Forcing and Response to Greenhouse Gases,
1059 Aerosols, and Ozone in CESM1." *Journal of Geophysical Research: Atmospheres* 124 (24): 13876–94.
1060 <https://doi.org/10.1029/2019JD030769>.
- 1061 Zhong, Y., A. Jahn, G. H. Miller, and A. Geirsdottir. 2018. "Asymmetric Cooling of the Atlantic and Pacific Arctic During
1062 the Past Two Millennia: A Dual Observation-Modeling Study." *Geophysical Research Letters* 45 (22): 12,497-
1063 12,505. <https://doi.org/10.1029/2018GL079447>.